Stable potassium (K) isotope characteristics at mid-ocean ridge hydrothermal vents and its 1 2 implications for the global K cycle 3 4 Xin-Yuan Zheng^{a,1}, Brian L Beard^b, Mason Neuman^b, Maria F Fahnestock^c, Julia G 5 Bryce^c, Clark M. Johnson^b 6 7 ^a Department of Earth and Environmental Sciences, University of Minnesota–Twin Cities, 116 8 Church Street SE, Minneapolis MN 55455, USA 9 ^b Department of Geoscience, University of Wisconsin–Madison, 1215 W Dayton Street, Madison 10 WI 53706, USA 11 ^c Department of Earth Sciences, University of New Hampshire, 56 College Road, NH 03824, 12 **USA** 13 14 Publisher version: 15 Zheng X.-Y., Beard B. L., Neuman M., Fahnestock M. F., Bryce J. G. and Johnson C. M. (2022) 16 Stable potassium (K) isotope characteristics at mid-ocean ridge hydrothermal vents and its 17 implications for the global K cycle. Earth and Planetary Science Letters 593, 117653, 18 https://doi.org/10.1016/j.epsl.2022.117653. 19 20 ¹ Corresponding author. E-mail address: zhengxy@umn.edu (X.-Y. Zheng)

Department of Earth and Environmental Sciences, University of Minnesota-Twin Cities, 150

John Tate Hall, 116 Church Street SE, Minneapolis MN 55455, USA

Phone: +1 612-301-3836

Abstract

21

22

23

24

25

26

27

28

29

30

31

32

33

34

35

36

37

38

39

40

41

42

43

Recent discoveries of significant variations in stable K isotope ratios (${}^{41}K/{}^{39}K$ or $\delta^{41}K$) among various terrestrial samples indicate that K isotopes can be a novel tracer for the global K cycle, but a key observation that seawater δ^{41} K is ~0.6% higher than the bulk silicate Earth remains unexplained. An unconstrained component critical to this puzzle is hydrothermal systems that represent both a major K source and sink in the ocean. Here we report δ^{41} K results on mid-ocean ridge (MOR) hydrothermal fluids from the Gorda Ridge and ~9°N East Pacific Rise (EPR), including time-series samples that recorded major perturbations in fluid chemistry induced by a local volcanic eruption. Fluid δ^{41} K values range from -0.46% to -0.15%, falling between those of fresh basalts and seawater. δ^{41} K values of "time-zero" fluids collected shortly after the volcanic eruption are shifted towards the seawater value, followed by a return to preeruption values within \sim 2 years. Fluid δ^{41} K variations are largely influenced by water–rock interactions, but they cannot be solely explained by simple mixing of seawater and K leached from basalts at high temperatures. Instead, these data imply small but significant isotope fractionation that enriches heavy K isotopes in basalts, likely caused by low-temperature alteration during the recharge stage of hydrothermal circulation. Our results preclude MOR hydrothermal systems as the cause for the heavy δ^{41} K value of seawater. Using fluid δ^{41} K data and K isotope fractionation constrained here for hydrothermal systems, a K mass-balance model implies a critical role for a marine sedimentary sink, possibly authigenic clay formation, in the global K cycle. Also, applying the K isotope fractionation constrained here to the published δ^{41} K data from ophiolites shows the possibility for significantly lower seawater δ^{41} K during the Ordovician, which can be explained by enhanced reverse weathering in response to distinct climate and tectonics at that time.

Keywords: potassium isotopes; hydrothermal fluid; potassium cycle; authigenic clay formation

45

46

47

48

49

50

51

52

53

54

55

56

57

58

59

60

61

62

63

64

65

66

44

1. Introduction

The stability of the global carbon cycle over the million-year timescale is closely related to destruction and neoformation of silicate minerals. Chemical breakdown of silicates sequesters atmospheric CO₂ and exports alkalinity and other soluble ions into the ocean. The effects of this so-called silicate weathering must be counterbalanced in the ocean to maintain the long-term stability of climate and seawater chemistry. Authigenic clay formation has been proposed as an important counterbalancing process (Mackenzie and Garrels, 1966; Isson and Planavsky, 2018). This putative process is often referred to as "reverse weathering" because the reaction involves formation of new clays *in-situ* in the ocean that consumes soluble cations and alkalinity, and releases CO₂. Increasingly, there is evidence to support clay formation under certain lowtemperature marine settings (e.g., Michalopoulos and Aller, 1995), but an unambiguous demonstration of its global significance remains lacking. The K cycle has unique bearing on the global silicate cycle, because K, the 4th most abundant cation in seawater, primarily resides in silicates rather than carbonates, making its geochemical cycle more directly coupled to silicate transformations relative to other major cations in seawater such as Mg and Ca. Recent studies have reported significant variations in stable K isotopes (${}^{41}\text{K}/{}^{39}\text{K}$ or $\delta^{41}\text{K}$) in terrestrial samples (e.g., Li et al., 2016; Wang and Jacobsen, 2016; Morgan et al., 2018; Wang et al., 2021b), providing a new proxy for the global K (hence silicate) cycle. For example, several studies have demonstrated the potential of K isotopes for tracing silicate weathering (Li et al., 2019a; Chen et al., 2020; Teng et al., 2020). Among these new studies, a particularly critical observation is that the seawater ⁴¹K/³⁹K ratio

that is \sim 0.6‰ heavier than the bulk silicate Earth (BSE). BSE has a narrow δ^{41} K range with an average value of \sim -0.45‰ (NIST 3141a scale) (e.g., Li et al., 2016; Wang and Jacobsen, 2016; Morgan et al., 2018; Huang et al., 2020), whereas seawater has a higher and homogenous δ^{41} K value of \sim 0.10‰ (e.g., Li et al., 2016; Wang and Jacobsen, 2016; Morgan et al., 2018).

The higher seawater δ^{41} K value compared to BSE remains unexplained, but it must be related to K isotope fractionation in one or more processes associated with K sources and sinks in the ocean. Potassium is added to seawater mainly through rivers and high-temperature hydrothermal fluids, and it is removed largely through low-temperature hydrothermal alteration and clay formation (e.g., Alt et al., 1986; Von Damm, 1995). The riverine input is unable to fully explain a seawater δ^{41} K value ~0.6‰ higher than BSE (Li et al., 2019a; Wang et al., 2021a). Authigenic clay formation, in principle, can be a viable contributor to the heavy seawater δ^{41} K because clays can preferentially retain light K isotopes based on field observations (Santiago Ramos et al., 2018; Li et al., 2019a). Direct field observations of reverse weathering, however, are challenging and often limited to marginal settings of considerable heterogeneity, making it difficult to assess its global significance.

Marine K isotope mass balance potentially provides a unique assessment for the global significance of authigenic clay formation. This approach avoids difficulties associated with extrapolation of spatially heterogeneous influence of clay formation to the global scale, but it requires constraints on K isotope characteristics associated with all other major K input and removal processes in the ocean. Hydrothermal systems are a key component in the global marine K cycle, but they are also one of the least constrained components in the marine K isotope mass balance. Hydrothermal alteration of oceanic crust is a seawater K sink at low temperature (< ~70°C), but a major K source at high temperature (e.g., Seyfried and Bischoff, 1979; Von

Damm, 1995). Potential K isotope fractionation during seawater–basalt interactions and emanations of K-rich hydrothermal fluids may, in principle, significantly affect seawater δ^{41} K, but modern hydrothermal systems have been rarely studied to date (Zheng et al., 2019). This work attempts to fill this critical gap through an investigation of K isotope characteristics in a suite of hydrothermal fluids collected from Pacific mid-ocean ridge (MOR) systems.

95

96

97

98

99

100

101

102

103

104

105

106

107

108

109

110

111

112

90

91

92

93

94

2. Sample background

Representative MOR hydrothermal fluids were studied here, including samples collected from three vents in the Sea Cliff hydrothermal field (Sea Cliff GR-14 Marker C, L, and Y) on the Gorda Ridge and three vents (Bio9, L, Medusa) on the East Pacific Rise (EPR) in the Pacific Ocean (Fig. S1 in Supplementary Material). The Sea Cliff hydrothermal field is located on the northernmost segment of the Gorda Ridge at ~42°N, and chemical compositions of fluids from this field were inferred to have been stable for ~20 years (Von Damm et al., 2006), making this location an ideal example for hydrothermal systems with long-term physicochemical stability. The samples used in this study had exit temperatures of ~300°C (Table S1 in Supplementary Material), with formation temperatures estimated to be >400°C (Von Damm et al., 2006). The EPR is an extensively studied fast spreading hydrothermal system (e.g., Fornari et al., 2012). Our samples include two time-series from two vents near $\sim 9^{\circ}50$ 'N (see sampling dates in Table S1); one suite was collected from the same orifice of the Bio9 vent, and the other one was from two immediately adjacent orifices of the L vent (L/La series). Measured exit temperatures of these samples ranged from 279°C to 386°C (Table S1), with estimated *in-situ* temperatures of >400°C at depths (Fornari et al., 2012). Our time-series bracketed a major volcanic eruption occurred between late 2005 and early 2006 that caused major changes in fluid chemistry (Fornari et al.,

2012). These samples, therefore, provide a unique opportunity to study possible transient evolution of fluid K isotopes in response to an eruptive perturbation. Fluids with exit temperatures of 335°C (Table S1) from the Medusa vent at an overlapping spreading center on the EPR at ~9°N were also analyzed in this study. Dregs precipitated during sampling (mostly sulfides) were not available for analysis, but it is unlikely that they could perceptibly affect fluid K isotopes because of generally high solubility of K salts and high K concentrations in fluids.

3. Methods

For K isotope analysis, aliquots of hydrothermal fluids containing $\sim \! 100~\mu g$ K were processed through Bio-Rad chromatographic columns packed with 2 ml AG50W–X8 cation exchange resin (200–400 mesh, H⁺ form). Potassium was separated from major matrix ions (e.g., Na, Mg, Ca) and quantitatively recovered from resin using 0.4 M HCl. The detailed elution protocol was provided in Supplementary Material Table S4. Total procedural blank was negligible ($\sim \! 20~ng$ K).

Potassium isotopes were analyzed on a collision-cell equipped MC-ICP-MS (*IsoProbe*) in the Department of Geoscience, University of Wisconsin-Madison, following the method reported in Li et al. (2016) with the exception that a desolvator was used in this study. Complete analytical details are provided in the Supplementary Material. Briefly, interferences on K isotopes from plasma-derived Ar species, notably ⁴⁰Ar¹H⁺ and the tailing of ⁴⁰Ar⁺, were reduced to a negligible level by using helium and deuterium as collision/reaction gases in a hexapole collision cell. Potassium isotopes were analyzed by a sample-standard bracketing protocol using an Aridus II desolvator. A pure K solution from High-Purity Standards was used as the

bracketing standard, and this solution was routinely analyzed against NIST SRM 3141a. All $\delta^{41}K$ data reported here were converted to the NIST SRM 3141a scale.

Quality of our K isotope analysis was evaluated through extensive tests using a series of in-house test solutions and reference materials, and accurate and precise $\delta^{41}K$ results were obtained in all tests (details in Supplementary Material). Our analyses yielded $\delta^{41}K$ values of -0.41 \pm 0.07% (2SD, n = 3) for BCR-2 and 0.10 \pm 0.05% (2SD, n = 3) for seawater, all of which agreed well with published values (Wang et al., 2021b). Despite being analyzed only once, BHVO-2 yielded a $\delta^{41}K$ value of -0.40% that also agreed with literature values (Wang et al., 2021b). Duplicate analyses of randomly selected fluid samples show that our $\delta^{41}K$ data can be reproduced \leq 0.05% (Table S1). Importantly, for 7 out of the total 11 individual sample collections studied here, aliquots from two different sampling bottles were intentionally analyzed to estimate reproducibility of endmember calculations; endmember $\delta^{41}K$ values calculated based on measurements of two individual bottles of the same vent all agreed \leq 0.02% (Fig. S3 in Supplementary Material).

Strontium was purified using Sr-Spec resin in 4 M HNO₃, and then recovered from the resin using 2% HNO₃. Total procedural blank was ~8 pg Sr, which was negligible compared to >70 ng Sr in each sample processed. Strontium isotopes (87 Sr/ 86 Sr) were analyzed on a VG Sector 54 thermal ionization mass spectrometer (TIMS) at University of Wisconsin-Madison, using Re filaments and a TaF₅ activator. Mass bias was corrected using an exponential law and 86 Sr/ 88 Sr = 0.1194. Analyses of NIST SRM-987 Sr standard and a marine carbonate standard EN-1 from the USGS yielded 87 Sr/ 86 Sr results of 0.710273 \pm 0.000016 (2SD, n = 10) and 0.709205 \pm 0.000005 (2SD, n = 4), respectively.

4. Results

158

159

160

161

162

163

164

165

166

167

168

169

170

171

172

173

174

175

176

177

178

179

180

Fluid K and Sr isotopes, along with other chemical compositions previously analyzed on the same samples, are provided in Supplementary Material Table S1. The estimated uncertainty for elemental concentrations is ~5% (1SD). Elemental concentrations in endmember fluids were calculated based on a conservative mixing of unadulterated seawater and pure hydrothermal fluids containing zero Mg (Supplementary Material Table S2). Isotope compositions of endmember fluids were obtained by extrapolating the measured and seawater isotope ratios against Mg/K ratios to Mg/K = 0 for K isotopes, and against Mg/Sr ratios to Mg/Sr = 0 for Sr isotopes (Supplementary Material Table S2). For one sample set, La.14, collected in 2006 soon after the 2005/2006 volcanic eruption, endmember δ^{41} K and 87 Sr/ 86 Sr values could not be precisely constrained because of large seawater entrainment (59-80 wt.%), and extremely low endmember [K] (0.4 mmol/kg) and [Sr] (~0) estimated for these fluids. Expectedly, the measured δ⁴¹K and ⁸⁷Sr/⁸⁶Sr values of these fluids were indistinguishable from seawater compositions. Hydrothermal fluids from EPR and the Gorda Ridge showed a wide range of chemical compositions (Fig. 1A–D). Endmember [C1] contents ranged from ~45 to 581 mmol/kg, representing ~8% to ~107% of the seawater [CI] concentration. Relative to seawater [K] of 10.1 mmol/kg (Von Damm, 2000), [K] in pure fluids ranged from an extremely depleted value of 0.4 mmol/kg found at the L site (La.14) soon after the volcanic eruption to enriched values of up to 24.2 mmol/kg at the Sea Cliff vent on the Gorda Ridge. Endmember δ^{41} K values varied between -0.46% and -0.15%. The estimated endmember fluid [Sr] contents, ranging between 0 and 82.1 μmol/kg at most vents, were lower than the ambient seawater level (87 μmol/kg, Von Damm, 2000), except for one sample from the L vent (L.13) before the 2005/2006 volcanic eruption that has a Sr concentration higher than seawater (i.e., 155.5 µmol/kg). Fluid ⁸⁷Sr/⁸⁶Sr ranged from

0.70319 to 0.70609. For time-series samples collected at Bio9 and L vents, fluid [K] and [Sr] decreased considerably soon after the volcanic eruption compared to pre-eruption levels, in concert with shifts in fluid $\delta^{41}K$ and ${}^{87}Sr/{}^{86}Sr$ towards the seawater values. Fluid concentrations and isotopic compositions of these two elements recovered at pre-eruption values over the following \sim 2 years.

5. Discussion

5.1 Controls on fluid chemistry

Potassium and other elemental concentrations in hydrothermal fluids are affected by phase separation that is the primary process known to significantly change fluid [Cl] contents in hydrothermal systems (e.g., German and Seyfried, 2014). This influence is evident from large variations in fluid [Cl] concentrations (Fig. 1). Two-phase separation was inferred to have occurred for the vents studied here (Von Damm, 2000; 2006; Foustoukos and Seyfried, 2007; Fornari et al., 2012). Most of our fluids derived from the vapor phase, as indicated by their low [Cl] relative to seawater (Fig. 1), with the only exception at the L site, where brine fluids were sampled outside the 2005/2006 volcanic eruption window. Because Cl is the major anion in hydrothermal fluids, differential partitioning of Cl into different phases produced by phase separation is accompanied by similar partitioning of cations, including K and Sr, to maintain charge balance (German and Seyfried, 2014). This explains the general positive correlation observed between cations (K and Sr) and Cl concentrations (Fig. 1A, C).

Besides phase separation, seawater–basalt interactions also affected fluid chemistry, as manifested in fluid K/Cl and ⁸⁷Sr/⁸⁶Sr ratios. Despite changes in absolute concentrations, two-phase separation generally does not change the K/Cl ratio in either of the two phases relative to

that of the initial solution (e.g., Berndt and Seyfried, 1990). However, except for samples collected shortly after the 2005/2006 volcanic eruption (L.14), all other fluids showed K excesses to varying degrees relative to K concentrations predicted based on fluid [CI] and the seawater K/Cl ratio (Fig. 1A), implying K additions in fluids from basalt. Our observation is consistent with laboratory experiments that demonstrated leaching of K from basalts by seawater at high temperatures (≥150°C) (Mottl and Holland, 1978; Seyfried and Bischoff, 1979). Fluid ⁸⁷Sr/⁸⁶Sr ratios provide further evidence for influence from seawater–basalt interactions. Distinct from fluid [Sr] contents that can be strongly mediated by formation of Sr-bearing minerals, notably anhydrite, fluid ⁸⁷Sr/⁸⁶Sr ratios are neither affected by mineral formation nor phase separation. Endmember fluid ⁸⁷Sr/⁸⁶Sr ratios fall within the range defined by seawater (~0.70916, Palmer and Edmond, 1989) and local basalts (~0.70245, Davis et al., 2008; Goss et al., 2010) (Fig. 1D), showing a clear influence from seawater–basalt interactions.

Time-series samples from Bio9 and L vents provide insights into the response of fluid chemistry to an eruptive perturbation. Consistent with observations from an earlier volcanic eruption in 1991 at EPR (Von Damm, 2000; 2004; Fornari et al., 2012), fluids collected soon after the 2005/2006 eruption (B9.20 and La.14), the so-called "time-zero" fluids, show extremely low [CI] (Fig. 1), reflecting phase separation at elevated temperature and shallow depth in response to rising magma. Identical to "time-zero" fluids from the 1991 eruption (Von Damm, 2000), B9.20 and La.14 fluids also have K/Cl ratios closer to the seawater ratio (Fig. 1A), implying a lesser influence of water–rock interaction on these samples. This is consistent with elevated ⁸⁷Sr/⁸⁶Sr in B9.20 fluid (Fig. 1D), although a similar inference based on Sr isotopes is not possible for La.14 samples that were estimated to be devoid of Sr in endmember fluids. The reduced influence of water–rock interaction may reflect heat-induced healing of rock fractures

that impeded exposure of rock surfaces to fluids, or a non-steady state condition where fluid recharge from fresh seawater occurred during the eruption. Nonetheless, chemical compositions of fluids, including Sr and K isotopes, returned to pre-eruption values within ~2 years after the eruption (Fig. 1), providing first-order evidence for the timescale over which changes of K isotopic compositions may occur in hydrothermal fluids.

5.2 K isotope compositions of MOR hydrothermal fluids

Our results provide the first glimpse of $\delta^{41}K$ values in marine hydrothermal fluids. Because seawater has a homogenous $\delta^{41}K$ value of ~0.10‰ (e.g., Li et al., 2016; Wang and Jacobsen, 2016; Morgan et al., 2018; Santiago Ramos et al., 2018), and basalts also show limited $\delta^{41}K$ variability with an average value of ~-0.45‰ (e.g., Li et al., 2016; Wang and Jacobsen, 2016; Morgan et al., 2018), endmember fluid $\delta^{41}K$ values that fall between seawater and basalt compositions (Fig. 1B) imply that K exchange during seawater–basalt interactions is the primary control on $\delta^{41}K$ values in MOR hydrothermal fluids.

A broadly positive correlation between fluid $\delta^{41}K$ and $^{87}Sr/^{86}Sr$ indicates the influence of seawater-basalt interaction (Fig. 1B, D); a higher $\delta^{41}K$ value (i.e., seawater-like) corresponds to higher $^{87}Sr/^{86}Sr$, indicative of less extensive seawater-basalt interaction, whereas the converse relation indicates higher extents of interaction. It is noted that fluid $\delta^{41}K$ values show a broadly negative correlation with fluid [Cl] (Fig. 1B). We, however, interpret this to be a coincidence rather than a causal link between $\delta^{41}K$ and phase separation, because the extent of seawater-basalt interaction also increases with fluid [Cl] for the suite of samples analyzed here, as indicated by a similarly negative correlation between fluid $^{87}Sr/^{86}Sr$ and [Cl] (Fig. 1D).

Further support for a major role of seawater–basalt interaction in controlling fluid $\delta^{41}K$ comes from the relation between fluid $\delta^{41}K$ and K excesses (Fig. 2). Net K gain (or loss) in a fluid sample, corrected for the effect of phase separation, can be quantified via the vertical "distance" of fluid [K] above (or below) the seawater K/Cl line in Fig. 1A, divided by the predicted seawater [K] at the corresponding fluid [Cl] on the seawater K/Cl line. We define this parameter as an enrichment factor (EF), where a negative value indicates net fluid K loss, and a positive value indicates net fluid K gain. All fluids exhibited varied K excesses (i.e., positive EF), except for the "time-zero" fluid La.14. Importantly, fluid $\delta^{41}K$ values are found to generally shift towards the basalt value with increasing K excesses (i.e., a larger EF value) (Fig. 2). This broad correlation implies that addition of varied amounts of basaltic K during seawater–basalt interaction is a main driver for fluid $\delta^{41}K$ variations.

5.3 Quantification of K isotope fractionation in hydrothermal systems

Despite the major influence of basaltic K addition, the occurrence of K isotope fractionation can be inferred when fluid δ^{41} K and K concentrations are considered together. Because fluid K excesses result from basaltic K addition, the relative K contributions from seawater and basalt in the fluid can be quantified for any given EF. Based on these contributions, a simple two-component mixing model, therefore, shows predicted fluid δ^{41} K in the absence of isotope fractionation. As shown in Fig. 2, however, observed fluid δ^{41} K values are consistently lower than the mixing line, indicating the occurrence of isotopic fractionation that favors light K isotopes in fluids. A complication of Fig. 2 lies in the fact that K enrichment factors are based on net fluid K excesses (or deficiencies) relative to seawater. Because K in seawater is lost to basalt during low-temperature hydrothermal alteration (Seyfried and Bischoff, 1979), K enrichment

factors referenced to seawater K concentration may underestimate the true proportion of K derived from basalts. As a result, fluid data in Fig. 2 may shift to higher enrichment factors, approaching the mixing line. One could estimate that removal of ~30% seawater K for Medusa vent, ~50% for Bio9 and L/La vents, and ~80% for Sea Cliff vent would be required to shift fluid data onto the mixing line. The exact percentage of K loss from seawater at the low-temperature recharge zone is not known, partly because of large uncertainties on the area of recharge zone. However, low-temperature hydrothermal fluids from two well-studied sites, Dorado outcrop at the Cocos Plate and Baby Bare on the flank of the Juan de Fuca Ridge, show only minor to moderate K depletion (~5% to 30%) relative to seawater (Wheat and Fisher, 2008). If these low-temperature fluids are representative of the fluid percolating through the low-temperature hydrothermal recharge zone in general, it is unlikely that our fluid data (except for the Medusa vent) could directly plot onto the seawater–basalt mixing line in Fig. 2, even though they may displace rightward slightly. We conclude, therefore, that K isotope fractionation that favors light K isotopes in fluids is the most plausible explanation.

The magnitude of K isotope fractionation can be quantified by an open-system water-rock interaction model similar to those previously developed to explain many other isotope systems (e.g., O, Li, Sr) in hydrothermal fluids and altered oceanic crust (e.g., Bowers and Taylor, 1985; Magenheim et al., 1995). In our model, fresh basalt is incrementally equilibrated with a chemically evolving fluid according to a K isotope fractionation factor $\Delta^{41}K_{fluid-basalt}$ ($\approx 10^3 ln\alpha_{fluid-basalt}$) along a single-pass flow. $\Delta^{41}K_{fluid-basalt}$ can be related to fluid $\delta^{41}K$ via the following equation (Derivation in Supplementary Material):

$$\delta^{41}K_{fluid} = \left(\delta^{41}K_{basalt} + \Delta^{41}K_{fluid-basalt}\right) - \left(\delta^{41}K_{basalt} - \delta^{41}K_{sw} + \Delta^{41}K_{fluid-basalt}\right) \exp^{\left(-\frac{D_K}{W/R}\right)}$$

(Eq. 1)

where $\delta^{41}K_{fluid}$, $\delta^{41}K_{basalt}$, and $\delta^{41}K_{sw}$ are the K isotope compositions of fluid, fresh basalt, and seawater, respectively; D_K is the distribution coefficient of K between basalt and fluid $([K]_{basalt}/[K]_{fluid})$; and W/R is the water/rock ratio involved in the interaction. The W/R ratio here is derived from fluid chemistry, and it is different from the physical water/rock ratio. Although Eq. (1) includes the partition coefficient that is traditionally defined for equilibrium conditions, the model does not constrain equilibrium K isotope fractionation factors or imply equilibrium fractionation because it adopts necessary simplification that ignores possible dependence of K isotope fractionation on temperature and mineralogy. Such dependence is currently poorly known in hydrothermal systems. Instead, the model is intended to provide first-order estimates on the net effect of K isotope fractionation (or "apparent" fractionation) induced during entire hydrothermal convection.

As shown in Eq. (1), a critical parameter needed to constrain $\Delta^{41}K_{fluid-basalt}$ is the W/R ratio. One method for estimating W/R relies on fluid K concentrations. Application of the same water-rock interaction model can yield the following relation between fluid K concentration and W/R ratio (details in Supplementary Material):

310
$$\frac{1}{(W/R)_K} = -\frac{1}{D_K} \ln \left(\frac{C_{basalt} - D_K C_{fluid}}{C_{basalt} - D_K C_{seawater}} \right) (Eq. 2)$$

where C_{basalt} , $C_{seawater}$, and C_{fluid} denote K concentrations in mid-ocean ridge basalt, seawater, and hydrothermal fluids. The principle of this method for W/R estimation is similar to the conventional approach that uses excess alkali metal concentrations in fluids relative to seawater and a box model (e.g., Von Damm et al., 1985), but our model is more realistic than a simple box model because it accounts for continuous reactions along the flow path. When a D_K value is given, Eqs. (1) and (2) together can quantify $\Delta^{41}K_{fluid-basalt}$.

Details on model parameter selection, along with sensitivity experiments that evaluated the influence of different parameter choices on the model output, are provided in the Supplementary Material. Conservative estimates from the model are shown in Fig. 3A, and these results yielded apparent K isotope fractionation ($\Delta^{41}K_{fluid-basalt}$) between \sim -0.1‰ and -0.6‰ for most samples. Larger K isotope fractionation of up to several per mil was constrained for fluids collected after the volcanic eruption (Fig. 3A), but it is most likely to be a spurious result due to an overestimate of W/R ratios in these samples, because their K concentrations are too close to seawater concentration on the Cl-normalized basis to be effective indicators of waterrock interactions. This is particularly evident from sample B9.20 whose K/Cl ratio is almost identical to seawater, but ⁸⁷Sr/⁸⁶Sr shows clear influence from basalt (Fig. 1A and D).

W/R estimation is almost always subject to uncertainty associated with incomplete knowledge on actual chemical reaction pathways that an element undergoes in a hydrothermal system (e.g., Berndt et al., 1988), and the uncertainty would in turn affect $\Delta^{41}K_{fluid-basalt} \text{ quantification. An alternative modelling approach that utilizes co-variations in fluid $^{87}\text{Sr}/^{86}\text{Sr}$ and $\delta^{41}\text{K}$ can provide a useful additional check. Compared to the K-only model, this approach takes advantage of the fact that <math>^{87}\text{Sr}/^{86}\text{Sr}$ is not affected by processes that could fractionate stable isotopes (e.g., temperature change and phase separation), but simply reflects mixing of Sr from seawater and basalt. Using a fractionation factor of zero for $^{87}\text{Sr}/^{86}\text{Sr}$, an equation similar to Eq. (1) can be written to describe the relation between fluid $^{87}\text{Sr}/^{86}\text{Sr}$ and W/R ratios:

337
$${}^{87}Sr/{}^{86}Sr_{fluid} = {}^{87}Sr/{}^{86}Sr_{basalt} - ({}^{87}Sr/{}^{86}Sr_{basalt} - {}^{87}Sr/{}^{86}Sr_{sw}) \exp^{\left(-\frac{D_{Sr}}{W/R}\right)}$$
 (Eq. 3)

where ${}^{87}Sr/{}^{86}Sr_{fluid}$, ${}^{87}Sr/{}^{86}Sr_{basalt}$, and ${}^{87}Sr/{}^{86}Sr_{sw}$ denote ${}^{87}Sr/{}^{86}Sr$ for fluid, fresh basalt,

and seawater, respectively; D_{Sr} is the Sr distribution coefficient.

Model parameter selection and sensitivity experiments that evaluated the influence of different input values are provided in detail in the Supplementary Material. Using reasonably chosen inputs, the coupled Sr–K isotope model provides conservative estimates on K isotope fractionation between ~ -0.2‰ and -0.5‰ (Fig. 3B), a range similar to that constrained from the K-only model. Ravizza et al. (2001) previously proposed the presence of a "non-zero Mg fluid" component that could have affected fluid chemistry at a few hydrothermal vents on EPR, based on a close examination of fluid ⁸⁷Sr/⁸⁶Sr and [Mg] relations in some fluid samples from 9°50'N, and they concluded that the estimated endmember ⁸⁷Sr/⁸⁶Sr for these vents could be lower than the true value. We do not have an extensive data set that allows for a similar examination, but, if the true endmember ⁸⁷Sr/⁸⁶Sr ratios were indeed higher than our current estimates, fluid data could shift to the right in Fig. 3B, implying even larger K isotope fractionation.

Apparent K isotope fractionation quantified from the two models agreed reasonably well (i.e., within \sim 0.4‰) for most samples, and the differences resulted from varied uncertainties in W/R estimation associated with each method. For several samples strongly affected by the volcanic eruption (Fig. 3), the magnitude of K isotope fractionation constrained by the K-only model is typically much larger than that constrained by the coupled Sr–K isotope model. Results from the latter model are favored because 87 Sr/ 86 Sr values in these samples are more sensitive to water–rock interactions than K concentrations (Fig. 1A and D). Regardless the absolute magnitude, both models imply uptake of heavy K isotopes in basalts, leaving fluids isotopically light. Our results provide the first quantification of K isotope fractionation in modern hydrothermal systems.

5.4 Possible controls on K isotope fractionation in hydrothermal systems

Although high-temperature hydrothermal fluids were analyzed in this study, their chemical compositions were affected by both low- and high-temperature reactions when seawater passed through the thermal gradient of the oceanic crust. Therefore, the fluids should record K isotope fractionation produced by any combination of phase separation, lowtemperature, and high-temperature alteration processes. Several useful inferences can be made regarding the relative significance of these three processes in producing the inferred apparent K isotope fractionation. First, results of our time-series samples indicate that phase separation is unlikely to be the main contributor to the inferred apparent isotope fractionation. B9.20 samples collected shortly after the volcanic eruption provide the best test among all fluids analyzed to evaluate the potential effect of phase separation on K isotope fractionation, apart from La.14 samples whose endmember δ^{41} K value cannot be precisely constrained. We focus on these samples because (1) they were least affected by water-rock interactions as indicated by their K/Cl and ⁸⁷Sr/⁸⁶Sr ratios (Fig. 1A, D); (2) given their extremely low [K], these vapor-phase fluids must represent small K reservoirs relative to their counterpart brines, and, hence, they should show the largest expression of phase-separation-induced isotope fractionation, if any, from a mass balance perspective. Considering more reliable results from the coupled Sr-K model for this particular sample, K isotope fractionation constrained by B9.20 is ~0.2‰ more negative than the isotopic fractionation constrained by fluids sampled from the same vent before the volcanic eruption (Fig. 3B), implying possible phase-separation-induced fractionation that favors light K isotopes in the vapor phase. The isotopic fractionation may be caused by a kinetic effect during phase separation because light K isotopes are known to diffuse faster than heavy K isotopes in aqueous solution (Bourg et al., 2010). However, although phase separation may fractionate K isotopes, the magnitude of fractionation is rather small as indicated by sample

363

364

365

366

367

368

369

370

371

372

373

374

375

376

377

378

379

380

381

382

383

384

B9.20. Its expression should be muted in more typical fluid samples that have much higher [K] (and [Cl]) concentrations based on a mass-balance consideration. Phase separation, therefore, cannot explain the apparent fractionation up to ~-0.6% constrained from our dataset.

386

387

388

389

390

391

392

393

394

395

396

397

398

399

400

401

402

403

404

405

406

407

408

Instead, K isotope fractionation is most likely to reflect isotopic partitioning between fluid and K-bearing minerals during hydrothermal alteration. Major K-bearing alteration products relevant to MOR hydrothermal systems studied here include mica- and smectite-group minerals (celadonite, nontronite, saponite), and occasionally K-feldspars, at low temperatures, and zeolites, mixed-layer chlorite-smectites, and chlorites at more elevated temperatures (Alt et al., 1986). Our inferred K isotope fractionation is consistent with an early study that showed preferential retainment of heavy K isotopes on zeolite upon chemical exchange with K solutions (Taylor and Urey, 1938). Also, mica group minerals (e.g., glauconite and muscovite), nonswelling clays (e.g., illite), and K-feldspars are inferred to preferentially retain heavy K isotopes based on analyses of natural samples, although smectites and chlorites were inferred to favor light K isotopes upon interactions with aqueous K (Santiago Ramos et al., 2018; Li et al., 2019a; Huang et al., 2020). Ab initio calculations suggest preferential enrichment of heavy K isotopes in muscovite and orthoclase relative to aqueous K, but they predict an enrichment of light K isotopes in illite (Zeng et al., 2019). A recent laboratory study suggested that the direction of K isotope fractionation may vary depending on whether K is adsorbed onto clay surfaces or incorporated into crystal lattices (Li et al., 2021). A coherent picture of direction and magnitude of K isotope fractionation between aqueous solution and different minerals remains lacking, so it is premature to estimate the relative importance of individual minerals in controlling K isotope fractionation in hydrothermal systems. Despite uncertainties, aqueous-mineral K isotope fractionation can certainly occur, providing a viable mechanism to explain our inferred K isotope fractionation. Our inference is consistent with a study on a non-marine hydrothermal system associated with a porphyry Cu deposit, where high $\delta^{41}K$ values were found in most alteration minerals (Li et al., 2019b).

Potassium is sequestered into basalt at low temperature ($< \sim 70$ °C), but strongly leached from basalt at high temperature (Seyfried and Bischoff, 1979; Von Damm, 1995). Previous studies on hydrothermal fluid chemistry at EPR have inferred almost quantitative extraction of K from basalts during high temperature alteration (Von Damm et al., 1985). Similarly, compared to the typical K₂O content of ~0.07 wt% in primary normal mid-ocean ridge basalt (Workman and Hart, 2005), consistently low K₂O contents of ~0.01 wt% measured in DSDP 504B core from the nearby East Pacific, below the volcanic zone of the altered oceanic crust, indicate leaching of over 85% K from primary basalt (Bach et al., 2003). Theoretically calculated K isotope fractionation between aqueous K and a variety of K-bearing minerals is typically ~0.5% or smaller around ~400°C (Zeng et al., 2019) – a temperature relevant to our study vents. Assuming a fractionation factor of 0.5% and 85% K loss from basalt, K leached from basalt at high temperatures should have a δ^{41} K value less than 0.1% different from the unaltered basalt value. In contrast, solution—mineral K isotope fractionation is estimated to be up to several per mil at low temperatures (Zeng et al., 2019). As a result, although fluids from high-temperature hydrothermal vents were analyzed, they are most likely to record K isotope fractionation at low temperature alteration during the downward limb of hydrothermal circulation, followed by mixing of variable amounts of basalt-derived K with δ^{41} K values similar to the pristine basalt.

429

430

409

410

411

412

413

414

415

416

417

418

419

420

421

422

423

424

425

426

427

428

5.5 Implications for the global K cycle in the modern ocean

Our inferred isotopic fractionation that favors light K isotopes in fluids precludes hydrothermal input as the cause for the high $\delta^{41}K$ value of seawater compared to BSE. Instead, preferential removal of heavy K isotopes from seawater in hydrothermal systems makes it more challenging to explain a high $\delta^{41}K$ value in seawater. Rivers, the other major K source in the ocean, also cannot fully explain the heavy K isotope signature in seawater (Li et al., 2019a; Wang et al., 2021a). These observations make it clear that invoking a marine sedimentary K sink for light K isotopes is required to explain the high $\delta^{41}K$ in seawater. Preferential loss of light K isotopes to sediments has been inferred based on marine porewater data (Santiago Ramos et al., 2018). A recent study showed that K sorption onto clay surfaces prefers heavy K isotopes (Li et al., 2021), an opposite direction of that required to explain the high seawater $\delta^{41}K$ value. Removal of light K isotopes to sediments is, therefore, most likely to require K incorporation into clay structures through clay formation processes. Our results highlight the significance of a marine sedimentary K sink, possibly through authigenic clay formation, in the global K cycle.

We may improve estimates of K fluxes in the global ocean using combined element and isotope mass balance equations – an approach first proposed by Li et al. (2019a):

$$F_{riv} + F_{MOR} = F_{alt} + F_{sed}$$
 (Eq. 4)

447
$$\delta^{41}K_{riv}F_{riv} + \delta^{41}K_{MOR}F_{MOR} = \delta^{41}K_{alt}F_{alt} + \delta^{41}K_{sed}F_{sed}$$
 (Eq. 5)

Eq. (4) describes that the total flux (F) of major K inputs in the ocean, including rivers (riv) and MOR hydrothermal fluids (MOR), is balanced by major K outputs, including a sedimentary sink (sed), most likely authigenic clay formation, and alteration of oceanic crust at low temperature (alt). Eq. (5) is the K isotope mass balance equation for the global ocean. Potassium isotope fractionation factors between seawater and the two outputs, Δ_{sw-sed} (= $\delta^{41}K_{sw} - \delta^{41}K_{sed}$) and Δ_{sw-alt}

453 (= $\delta^{41}K_{sw} - \delta^{41}K_{alt}$), can be introduced to replace $\delta^{41}K_{sed}$ and $\delta^{41}K_{alt}$ in Eq. (5). Then, Eqs. (4) and 454 (5) yield:

455
$$\delta^{41}K_{sw} = \frac{1}{1+A}\delta^{41}K_{riv} + \frac{A}{1+A}\delta^{41}K_{MOR} + \frac{B}{1+B}\Delta_{sw-alt} + \frac{1}{1+B}\Delta_{sw-sed}$$
(Eq. 6)

where A and B represent flux ratio F_{MOR}/F_{riv} and F_{alt}/F_{sed} , respectively.

456

457

458

459

460

461

462

463

464

465

466

467

468

469

470

471

472

473

474

475

The estimated global riverine input ($\delta^{41}K_{riv}$) ranges between -0.22% and -0.38% (Li et al., 2019a; Wang et al., 2021a). Excluding the "time-zero" fluids collected under a likely nonsteady state condition immediately after the volcanic eruption (B9.20 and La.14), other fluids analyzed in this study gave an average δ^{41} K value of -0.32 \pm 0.08% (1SD). Given that these fluids cover a spread of K concentrations from seawater-like to more concentrated values typical of MOR fluids in the global ocean, we consider the average δ^{41} K value to be a reasonable representation of the global MOR input ($\delta^{41}K_{MOR}$). Fluids with considerably higher K concentrations do exist, but the presence of these fluids should only drive the global δ^{41} K average towards the basalt composition because of excessive addition of isotopically unfractionated K from leaching of basalt at high temperatures, as constrained by mass balance. As discussed in Section 5.4, although high-temperature hydrothermal fluids were studied here, our inferred K isotope fractionation should mostly represent fractionation produced by waterrock interaction at low temperature, providing estimates for $\Delta_{\text{sw-alt}}$. It is important to note that the expression of this K isotope fractionation is muted in high-temperature fluids due to mixing of basaltic K at high temperatures, but this fractionation cannot be ignored because large lowtemperature hydrothermal reaction zones represent a major but under-sampled K sink in the global ocean. Low-temperature hydrothermal fluids, such as those from Dorado and Baby Bare sites (Wheat and Fisher, 2008), are expected to be critical future tests for our inferred K isotope fractionation.

Previous estimates of K input and output fluxes were associated with large uncertainties, with estimated F_{MOR} , F_{sed} , F_{riv} , and F_{alt} fluxes ranging from 5 to 36 Tg/yr, from 25 to 52 Tg/yr, from 52 to 62 Tg/yr, and from 12 to 15.6 Tg/yr, respectively (see Li et al., 2019a and references therein). Using our new results on $\delta^{41}K_{MOR}$ and Δ_{sw-alt} , two billion Monte Carlo simulations were conducted to screen the full ranges of previous estimates for all parameters in Eqs. (4) and (5) (details in Supplementary Material). The results showed that estimates of F_{MOR} and F_{sed} fluxes can be considerably refined (Fig. 4A and B), yielding a narrower range between 5 and 15.3 Tg/yr for F_{MOR} , and between 42 to 52 Tg/yr for F_{sed} . F_{riv} and F_{alt} are not sensitive to the model, so they cannot be further refined.

The key observation here is that the refined F_{sed} flux occupied the upper range of previous estimates, implying that the role of this removal process in the global K cycle is more important than previously considered. This tendency stays true even if a higher F_{alt} upper limit is used as the model input based on recent suggestions for a possible larger F_{alt} in the global ocean (details in Supplementary Material), although absolute values for F_{MOR} and F_{sed} can change. This highlights the need to improve the F_{alt} estimate in the future. The model also shows that any refined F_{riv} and F_{alt} estimates in future via other approaches could further improve F_{MOR} and F_{sed} estimates, because these fluxes are intimately linked through K element and isotope massbalance relations. In addition, our results show that the global average K isotope fractionation associated with the sedimentary source Δ_{sw-sed} can be refined by this model. Under the current model inputs, a narrow range of 0.53 \pm 0.06% (1 SD) was obtained, even though an exceptionally large initial input range between -3% and +3% was tested in our simulations (Fig. 4C). This fractionation lies within previous estimates between 0% and 2% based on local field

observations (Santiago Ramos et al., 2018; Li et al., 2019a), and such an estimate can be useful in future model efforts focused on the K isotope mass balance of the global ocean.

500

501

502

503

504

505

506

507

508

509

510

511

512

513

514

515

516

517

518

519

520

498

499

5.6 Implications for δ^{41} K of ancient seawater

Our results have implications for interpreting δ^{41} K data from ophiolites. Ophiolites preserve records of ancient hydrothermal alteration and, hence, potentially δ^{41} K values of ancient seawater. A few studies have reported δ^{41} K data from several ophiolites, or altered oceanic crust, with ages ranging from the Cretaceous to Ordovician, and these studies generally argued for either no K isotope fractionation during hydrothermal circulation or enrichment of light K isotopes in altered basalts (Parendo et al., 2017; Hu et al., 2020; Santiago Ramos et al., 2020). Previous interpretations, however, often hinged on the assumption of ancient seawater δ^{41} K at the time of alteration. For example, based on a water-rock interaction model similar to our Sr-K isotope model and an assumption that Ordovician seawater had the same $\delta^{41}K$ value as modern seawater, a reasonable choice at the time of study, $\delta^{41}K$ data from ~485 Ma Bay of Islands (BOI) ophiolite were interpreted to reflect uptake of seawater K in basalts with negligible K isotope fractionation (Parendo et al., 2017). However, because our study provides direct estimates on $\Delta^{41}K_{fluid-basalt}$, we can invert the use of the water-rock interaction model to infer Ordovician seawater δ^{41} K. Using the same model and input parameters adopted in Parendo et al. (2017), but replacing their $\Delta^{41}K_{fluid-basalt}$ with a conservative estimate of -0.2% from this study, we show that an Ordovician seawater δ^{41} K value ~0.3% lower than today is required to fit the K and Sr isotope data reported for BOI ophiolite (Fig. 5).

A lower Ordovician seawater $\delta^{41}K$ value is consistent with climatic and tectonic conditions at that time. The Ordovician was generally considered to have had high atmospheric

pCO₂ levels up to ~10-time higher than at present (e.g., Berner and Kothavala, 2001; Lenton et al., 2018), causing more intensive silicate weathering (e.g., Avigad et al., 2005). This would drive $\delta^{41}K_{riv}$ closer to that of unaltered basalts, based on the negative relation observed between river-water δ^{41} K and weathering intensity (Li et al., 2019a). The Ordovician was also associated with a high ocean crust production rate ~2 times of the modern level (Gaffin, 1987), which is consistent with a high sea level at the time (Miller et al., 2005). Faster production of ocean crust may cause more intense high-temperature hydrothermal alteration that should shift $\delta^{41}K_{MOR}$ closer to unaltered basalts, and it may also create larger areas for low-temperature hydrothermal alteration. The F_{MOR}/F_{riv} ratio in the Ordovician ocean was inferred to be ~22% higher than that in the modern ocean (Hardie, 1996). Based on mass-balance Eq. (6), assuming both $\delta^{41}K_{riv}$ and $\delta^{41}K_{MOR}$ to be an igneous rock value, a ~22% higher F_{MOR}/F_{riv} ratio, and the same K isotope fractionation factors as today, a ~0.3% lower $\delta^{41}K_{sw}$ would require a ~25% decrease in the F_{alt}/F_{sed} ratio in the Ordovician ocean relative to today. If F_{alt} can be directly scaled with the ~2time increase in the ocean crust production rate during the Ordovician, a ~25% decrease in F_{alt}/F_{sed} requires a ~1.7-time increase in F_{sed} relative to the modern level. Because occurrence of authigenic clay formation is probably most intensive at continental margins where the supply of soluble cations required for the reaction are the most abundant (e.g., Michalopoulos and Aller, 1995), an increase in F_{sed} in the Ordovician is most likely explained by enhanced reverse weathering at continental margins whose areas increased significantly during high sea-level stands in the Ordovician (Miller et al., 2005). A lower seawater δ^{41} K value in the early Ordovician ocean, therefore, implies enhanced reverse weathering. Certainly, complications may include the applicability of modern hydrothermal systems to ancient ophiolites, as well as possible later alteration of isotope signatures during obduction and preservation of ophiolites.

521

522

523

524

525

526

527

528

529

530

531

532

533

534

535

536

537

538

539

540

541

542

Nonetheless, our results highlight the possibility that seawater $\delta^{41}K$ may have varied over geologic time. Further understanding of ancient seawater $\delta^{41}K$ is of considerable significance because changes in the marine K cycle can ultimately provide valuable clues to understanding of the long-term variations in the global carbon cycle.

6. Conclusions

A suite of mid-ocean ridge hydrothermal fluids collected from the Pacific show $\delta^{41}K$ values between -0.46% and -0.15%. Although these $\delta^{41}K$ values span the range between seawater and basalt, the observed K isotope variability cannot be explained by a simple mixing of the two endmembers when fluid [K] concentrations are considered. Instead, $\delta^{41}K$ –[K] variations require K isotope fractionation that favors light K isotopes in fluids. The magnitude of apparent K isotope fractionation can be estimated to range from ~-0.2% and -0.6%. This apparent K isotope fractionation is most likely to reflect fractionation produced during low-temperature alteration, rather than phase separation or high-temperature alteration. Potassium isotope fractionation and fluid $\delta^{41}K$ values constrained here demonstrate the necessity to invoke a sedimentary sink, possibly authigenic clay formation, to explain the high $\delta^{41}K$ value of seawater. Our results also highlight that a different $\delta^{41}K$ value of ancient seawater remains a viable possibility that requires further tests but has important bearing for understanding of $\delta^{41}K$ data in ophiolites and the past global carbon cycle.

Acknowledgements

This work was supported by NSF Award 1741048 to BLB, CMJ, and XZ. XZ would like to thank Prof. Bill Seyfried (University of Minnesota) for helpful discussion, and Prof. Zhimian

- Cao (Xiamen University) for providing the natural seawater sample used as an in-house K
- isotope standard in this study. We thank two anonymous reviewers for their constructive
- comments and editorial handling by Prof. Frédéric Moynier.

References

- Alt J. C., Honnorez J., Laverne C. and Emmermann R. (1986) Hydrothermal alteration of a 1 km section through the upper oceanic crust, Deep Sea Drilling Project Hole 504B:
 Mineralogy, chemistry and evolution of seawater-basalt interactions. *Journal of Geophysical Research: Solid Earth* 91, 10309-10335, 10.1029/JB091iB10p10309.
- Avigad D., Sandler A., Kolodner K., Stern R. J., McWilliams M., Miller N. and Beyth M. (2005)
 Mass-production of Cambro–Ordovician quartz-rich sandstone as a consequence of
 chemical weathering of Pan-African terranes: Environmental implications. *Earth and*Planetary Science Letters 240, 818-826, https://doi.org/10.1016/j.epsl.2005.09.021.
 - Bach W., Peucker-Ehrenbrink B., Hart S. R. and Blusztajn J. S. (2003) Geochemistry of hydrothermally altered oceanic crust: DSDP/ODP Hole 504B Implications for seawater-crust exchange budgets and Sr- and Pb-isotopic evolution of the mantle. *Geochemistry, Geophysics, Geosystems* **4**, 10.1029/2002gc000419.
 - Berndt M. E. and Seyfried W. E. (1990) Boron, bromine, and other trace elements as clues to the fate of chlorine in mid-ocean ridge vent fluids. *Geochimica et Cosmochimica Acta* **54**, 2235-2245, https://doi.org/10.1016/0016-7037(90)90048-P.
 - Berndt M. E., Seyfried W. E. and Beck J. W. (1988) Hydrothermal alteration processes at midocean ridges: Experimental and theoretical constraints from Ca and Sr exchange reactions and Sr isotopic ratios. *Journal of Geophysical Research: Solid Earth* **93**, 4573-4583, 10.1029/JB093iB05p04573.
 - Berner R. A. and Kothavala Z. (2001) Geocarb III: A Revised Model of Atmospheric CO2 over Phanerozoic Time. *Am. J. Sci.* **301**, 182-204, 10.2475/ajs.301.2.182.
 - Bourg I. C., Richter F. M., Christensen J. N. and Sposito G. (2010) Isotopic mass dependence of metal cation diffusion coefficients in liquid water. *Geochimica et Cosmochimica Acta* **74**, 2249-2256, https://doi.org/10.1016/j.gca.2010.01.024.
 - Bowers T. S. and Taylor H. P. (1985) An integrated chemical and stable-isotope model of the origin of Midocean Ridge Hot Spring Systems. *Journal of Geophysical Research: Solid Earth* **90**, 12583-12606, 10.1029/JB090iB14p12583.
 - Chen H., Liu X.-M. and Wang K. (2020) Potassium isotope fractionation during chemical weathering of basalts. *Earth and Planetary Science Letters* **539**, 116192, https://doi.org/10.1016/j.epsl.2020.116192.
- Davis A. S., Clague D. A., Cousens B. L., Keaten R. and Paduan J. B. (2008) Geochemistry of basalt from the North Gorda segment of the Gorda Ridge: Evolution toward ultraslow spreading ridge lavas due to decreasing magma supply. *Geochemistry, Geophysics, Geosystems* 9, 10.1029/2007GC001775.
- Fornari D. J., Von Damm K. L., Bryce J. G., Cowen J. P., Ferrini V., Fundis A., Lilley M. D., LUTHER III G. W., Mullineaux L. S. and Perfit M. R. (2012) The East Pacific Rise

between 9 N and 10 N: Twenty-five years of integrated, multidisciplinary oceanic spreading center studies. *Oceanography* **25**, 18-43,

619

620

621 622

623

627

628

632

633

634

635

636

637 638

639

640

641

- Foustoukos D. I. and Seyfried W. E. (2007) Quartz solubility in the two-phase and critical region of the NaCl–KCl–H2O system: Implications for submarine hydrothermal vent systems at 9° 50′ N East Pacific Rise. *Geochimica et Cosmochimica Acta* **71**, 186-201, https://doi.org/10.1016/j.gca.2006.08.038.
- Gaffin S. (1987) Ridge volume dependence on seafloor generation rate and inversion using long term sealevel change. *Am. J. Sci.* **287**, 596-611, 10.2475/ajs.287.6.596.
- 616 German C. R. and Seyfried W. E. (2014) Hydrothermal processes. In *Treatise on Geochemistry*617 (Second Edition) (eds. H. D. Holland and K. K. Turekian.) Elsevier, Oxford. pp. 191-233,
 618 https://doi.org/10.1016/B978-0-08-095975-7.00607-0.
 - Goss A. R., Perfit M. R., Ridley W. I., Rubin K. H., Kamenov G. D., Soule S. A., Fundis A. and Fornari D. J. (2010) Geochemistry of lavas from the 2005-2006 eruption at the East Pacific Rise, 9° 46′ N-9° 56′ N: Implications for ridge crest plumbing and decadal changes in magma chamber compositions. *Geochemistry, Geophysics, Geosystems* 11, doi:10.1029/2009GC002977.
- Hardie L. A. (1996) Secular variation in seawater chemistry: An explanation for the coupled secular variation in the mineralogies of marine limestones and potash evaporites over the past 600 m.y. *Geology* **24**, 279-283, 10.1130/0091-7613(1996)024<0279:svisca>2.3.co;2.
 - Hu Y., Teng F.-Z., Plank T. and Chauvel C. (2020) Potassium isotopic heterogeneity in subducting oceanic plates. *Science Advances* **6**, eabb2472, 10.1126/sciadv.abb2472.
- Huang T.-Y., Teng F.-Z., Rudnick R. L., Chen X.-Y., Hu Y., Liu Y.-S. and Wu F.-Y. (2020)
 Heterogeneous potassium isotopic composition of the upper continental crust.
 Geochimica et Cosmochimica Acta 278, 122-136, 10.1016/j.gca.2019.05.022.
 - Isson T. T. and Planavsky N. J. (2018) Reverse weathering as a long-term stabilizer of marine pH and planetary climate. *Nature* 10.1038/s41586-018-0408-4.
 - Lenton T. M., Daines S. J. and Mills B. J. W. (2018) COPSE reloaded: An improved model of biogeochemical cycling over Phanerozoic time. *Earth-Science Reviews* **178**, 1-28, https://doi.org/10.1016/j.earscirev.2017.12.004.
 - Li S., Li W., Beard B. L., Raymo M. E., Wang X., Chen Y. and Chen J. (2019a) K isotopes as a tracer for continental weathering and geological K cycling. *Proceedings of the National Academy of Sciences* 201811282, 10.1073/pnas.1811282116.
 - Li W., Beard B. L. and Li S. (2016) Precise measurement of stable potassium isotope ratios using a single focusing collision cell multi-collector ICP-MS. *Journal of Analytical Atomic Spectrometry* **31**, 1023-1029, 10.1039/C5JA00487J.
- 643 Li W., Liu X.-M., Hu Y., Teng F.-Z. and Hu Y. (2021) Potassium isotopic fractionation during 644 clay adsorption. *Geochimica et Cosmochimica Acta* **304**, 160-177, 645 https://doi.org/10.1016/j.gca.2021.04.027.
- Li W., Zhao S., Wang X., Li S., Wang G., Yang T. and Jin Z. (2019b) Fingerprinting
 hydrothermal fluids in porphyry Cu deposits using K and Mg isotopes. *Science China Earth Sciences* 10.1007/s11430-018-9387-2.
- Mackenzie F. T. and Garrels R. M. (1966) Chemical mass balance between rivers and oceans.
 Am. J. Sci. 264, 507-525, 10.2475/ajs.264.7.507.
- Magenheim A. J., Spivack A. J., Alt J. C., Bayhurst G., Chan L., Zuleger E. and Gieskes J. M. (1995) Borehole fluid chemistry in Hole 504b, Leg 137: formation water or in-situ reaction?, Proceedings of the Ocean Drilling Program, Scientific Results, pp. 141-52.

- Michalopoulos P. and Aller R. C. (1995) Rapid Clay Mineral Formation in Amazon Delta Sediments: Reverse Weathering and Oceanic Elemental Cycles. *Science* **270**, 614-617, 10.1126/science.270.5236.614.
- Miller K. G., Kominz M. A., Browning J. V., Wright J. D., Mountain G. S., Katz M. E.,
 Sugarman P. J., Cramer B. S., Christie-Blick N. and Pekar S. F. (2005) The Phanerozoic
 Record of Global Sea-Level Change. *Science* 310, 1293-1298, 10.1126/science.1116412.
- Morgan L. E., Santiago Ramos D. P., Davidheiser-Kroll B., Faithfull J., Lloyd N. S., Ellam R.
 M. and Higgins J. A. (2018) High-precision ⁴¹K/³⁹K measurements by MC-ICP-MS indicate terrestrial variability of δ⁴¹K. *Journal of Analytical Atomic Spectrometry* 33, 175-186, 10.1039/C7JA00257B.
- Mottl M. J. and Holland H. D. (1978) Chemical exchange during hydrothermal alteration of basalt by seawater—I. Experimental results for major and minor components of seawater.

 Geochimica et Cosmochimica Acta 42, 1103-1115, http://dx.doi.org/10.1016/0016-7037(78)90107-2.
- Palmer M. R. and Edmond J. M. (1989) The strontium isotope budget of the modern ocean.

 Earth and Planetary Science Letters 92, 11-26, http://dx.doi.org/10.1016/0012-821X(89)90017-4.
- Parendo C. A., Jacobsen S. B. and Wang K. (2017) K isotopes as a tracer of seafloor hydrothermal alteration. *Proc Natl Acad Sci U S A* **114**, 1827-1831, 10.1073/pnas.1609228114.

674

675 676

677

678 679

680

681

682 683

684

685

686 687

- Ravizza G., Blusztajn J., Von Damm K. L., Bray A. M., Bach W. and Hart S. R. (2001) Sr isotope variations in vent fluids from 9° 46′ -9° 54′ N East Pacific Rise: evidence of a non-zero-Mg fluid component. *Geochimica et Cosmochimica Acta* **65**, 729-739, https://doi.org/10.1016/S0016-7037(00)00590-1.
- Santiago Ramos D. P., Morgan L. E., Lloyd N. S. and Higgins J. A. (2018) Reverse weathering in marine sediments and the geochemical cycle of potassium in seawater: Insights from the K isotopic composition (⁴¹K/ ³⁹K) of deep-sea pore-fluids. *Geochimica et Cosmochimica Acta* **236**, 99-120, 10.1016/j.gca.2018.02.035.
- Santiago Ramos D. P., Coogan L. A., Murphy J. G. and Higgins J. A. (2020) Low-temperature oceanic crust alteration and the isotopic budgets of potassium and magnesium in seawater. *Earth and Planetary Science Letters* **541**, 116290, https://doi.org/10.1016/j.epsl.2020.116290.
- Seyfried W. E. and Bischoff J. L. (1979) Low temperature basalt alteration by sea water: an experimental study at 70°C and 150°C. *Geochimica et Cosmochimica Acta* **43**, 1937-1947, http://dx.doi.org/10.1016/0016-7037(79)90006-1.
- Taylor T. I. and Urey H. C. (1938) Fractionation of the Lithium and Potassium Isotopes by Chemical Exchange with Zeolites. *The Journal of Chemical Physics* **6**, 429-438, 10.1063/1.1750288.
- Teng F.-Z., Hu Y., Ma J.-L., Wei G.-J. and Rudnick R. L. (2020) Potassium isotope fractionation during continental weathering and implications for global K isotopic balance. *Geochimica et Cosmochimica Acta* 278, 261-271,

 https://doi.org/10.1016/j.gca.2020.02.029.
- Von Damm K. (1995) Controls on the chemistry and temporal variability of seafloor hydrothermal fluids. *Seafloor hydrothermal systems: Physical, chemical, biological, and* geological interactions **91**, 222-247,

- Von Damm K. L. (2000) Chemistry of hydrothermal vent fluids from 9°–10°N, East Pacific Rise: "Time zero," the immediate posteruptive period. *Journal of Geophysical Research:*Solid Earth **105**, 11203-11222, doi:10.1029/1999JB900414.
- Von Damm K. L. (2004) Evolution of the hydrothermal system at East Pacific Rise 9 50 N:
 geochemical evidence for changes in the upper oceanic crust. *Mid Ocean Ridges* 285-304,

- Von Damm K. L., Edmond J. M., Grant B., Measures C. I., Walden B. and Weiss R. F. (1985) Chemistry of submarine hydrothermal solutions at 21 °N, East Pacific Rise. *Geochimica et Cosmochimica Acta* **49**, 2197-2220, https://doi.org/10.1016/0016-7037(85)90222-4.
- Von Damm K. L., Parker C. M., Lilley M. D., Clague D. A., Zierenberg R. A., Olson E. J. and McClain J. S. (2006) Chemistry of vent fluids and its implications for subsurface conditions at Sea Cliff hydrothermal field, Gorda Ridge. *Geochemistry, Geophysics, Geosystems* 7, 10.1029/2005GC001034.
- Wang K. and Jacobsen S. B. (2016) An estimate of the Bulk Silicate Earth potassium isotopic composition based on MC-ICPMS measurements of basalts. *Geochimica et Cosmochimica Acta* **178**, 223-232, http://dx.doi.org/10.1016/j.gca.2015.12.039.
- Wang K., Peucker-Ehrenbrink B., Chen H., Lee H. and Hasenmueller E. A. (2021a) Dissolved potassium isotopic composition of major world rivers. *Geochimica et Cosmochimica Acta* **294**, 145-159, https://doi.org/10.1016/j.gca.2020.11.012.
 - Wang K., Li W., Li S., Tian Z., Koefoed P. and Zheng X.-Y. (2021b) Geochemistry and cosmochemistry of potassium stable isotopes. *Geochemistry* 125786, https://doi.org/10.1016/j.chemer.2021.125786.
 - Wheat C. G. and Fisher A. T. (2008) Massive, low-temperature hydrothermal flow from a basaltic outcrop on 23 Ma seafloor of the Cocos Plate: Chemical constraints and implications. *Geochem. Geophys. Geosyst.* **9**, 10.1029/2008gc002136.
- Workman R. K. and Hart S. R. (2005) Major and trace element composition of the depleted MORB mantle (DMM). *Earth and Planetary Science Letters* **231**, 53-72, https://doi.org/10.1016/j.epsl.2004.12.005.
- Zeng H., Rozsa V. F., Nie N. X., Zhang Z., Pham T. A., Galli G. and Dauphas N. (2019) Ab
 Initio Calculation of Equilibrium Isotopic Fractionations of Potassium and Rubidium in
 Minerals and Water. ACS Earth and Space Chemistry 3, 2601-2612,
 10.1021/acsearthspacechem.9b00180.
- Zheng X.-Y., Beard B. L., Neuman M., Fahnestock M. F., Bryce J. G. and Johnson C. M. (2019)
 Constraining Stable K Isotope Mass Balance of the Global Ocean and Its Implications for
 the Modern and Past Silicate Cycle. *AGU Fall Meeting Abstracts* EP33C-2361,
 734

(Color figures are required only for the online version, but is not required in print)

2

4

5

6

7

8

9

10

11

12

13

14

15

16

17

1

Fig 1. Endmember (EM) concentrations and isotope compositions for the fluids analyzed in this study, calculated based on the assumption that endmember fluids were Mg-free: (A) [K] concentrations; (B) δ^{41} K; (C) [Sr] concentrations; (D) 87 Sr/ 86 Sr. Bio9 and L/La were collected as time-series samples with larger numbers in their sample names corresponding to more recent sampling. Samples B9.20 and La.14 were collected soon after the 2005/2006 volcanic eruption in 2006. Endmember δ^{41} K and 87 Sr/ 86 Sr cannot be precisely constrained for La.14 due to the presence of high Mg in the sample indicative of entrainment of a large seawater component (>60%) during sampling, so the measured rather than endmember values were plotted and indicated by a question mark for this sample. Seawater [C1], [K], and [Sr] concentrations were taken from Von Damm (2000). Seawater δ^{41} K composition was based on the average of the data reported in literature (Li et al., 2016; Wang and Jacobsen, 2016; Morgan et al., 2018; Santiago Ramos et al., 2018), and seawater ⁸⁷Sr/⁸⁶Sr was taken from Palmer and Edmond (1989). Endmember basalt δ^{41} K composition was based on the average of the basalt data reported in literature (Li et al., 2016; Wang and Jacobsen, 2016; Morgan et al., 2018), and basalt 87Sr/86Sr was based on data reported for MORB samples collected near our study areas (Davis et al., 2008;

19

20

21

22

23

18

Goss et al., 2010).

Fig 2. Endmember (EM) δ^{41} K values of the fluids plotted against fluid K enrichment factor (EF) – a parameter that quantifies K excesses in fluids relative to the expected seawater K contents at corresponding fluid [CI] concentrations. Endmember δ^{41} K value cannot be precisely constrained for La.14 due to entrainment of a large seawater component (>60%) during sampling, so the

measured $\delta^{41}K$ value was plotted for this sample with a question mark. The dashed line is the simple two-component mixing line between seawater- and basalt-derived K based on their relative contributions in the fluid at the given [K] enrichment factor. This mixing line represents the expected fluid $\delta^{41}K$ values in the absence of K isotope fractionation. The fact that all our observed endmember fluid $\delta^{41}K$ values fall below the mixing line implies the occurrence of K isotope fractionation that favors light K isotopes in fluids in hydrothermal processes. Seawater $\delta^{41}K$ composition was based on the average of the data reported in literature (Li et al., 2016; Wang and Jacobsen, 2016; Morgan et al., 2018; Santiago Ramos et al., 2018), and basalt $\delta^{41}K$ composition was based on the average of the basalt data reported in literature (Li et al., 2016; Wang and Jacobsen, 2016; Morgan et al., 2018).

Fig 3. Modeled apparent K isotope fractionation factors using (A) the K-only model that relied on fluid [K] concentrations to estimate water/rock ratios, and (B) a coupled K–Sr isotope model that relied on fluid 87 Sr/ 86 Sr to infer water/rock ratios. Blue lines in both plots are model outputs using different K isotope fractionation factors ($\Delta_{fluid-basalt}$) with 0.2% increments. Endmember fluid compositions obtained from this study were plotted against the model outputs. The subtle differences in the K isotope fractionation factors constrained from the two models reflect the intrinsic uncertainties in estimation of water/rock ratios associated with each method. For Bio9 and L/La time-series samples collected after the 2005/2006 volcanic eruption, especially those with extremely low [K] concentrations (i.e., B9.20 and La.14), the K-only model cannot effectively estimate their water/rock ratios. Consequently, the resultant K isotope fractionation factors for these samples from the K-only model are not reliable compared to the coupled K-Sr isotope model. Seawater endmember δ^{41} K composition was based on the average of the data

47 reported in literature (Li et al., 2016; Wang and Jacobsen, 2016; Morgan et al., 2018; Santiago Ramos et al., 2018), and seawater ⁸⁷Sr/⁸⁶Sr was taken from Palmer and Edmond (1989). 48 Endmember basalt δ^{41} K composition was based on the average of the basalt data reported in 49 literature (Li et al., 2016; Wang and Jacobsen, 2016; Morgan et al., 2018), and basalt ⁸⁷Sr/⁸⁶Sr 50 51 was based on data reported for MORB samples collected near our study areas (Davis et al., 2008; 52 Goss et al., 2010). 53 54 Fig 4. Results of 2 billion Monte Carlo simulations for the combined K elemental and isotopic 55 mass balance model for the global ocean. This coupled model includes two K source flux terms, 56 namely riverine and mid-ocean ridge hydrothermal inputs (F_{riv} and F_{MOR}), two K sink flux terms, 57 including low-temperature hydrothermal alteration and a sedimentary sink that is likely to be 58 authigenic clay formation (Falt and Fsed), and two K isotope fractionation factors associated with 59 low-temperature alteration and the sedimentary sink ($\Delta_{\text{sw-alt}}$ and $\Delta_{\text{sw-sed}}$). The prescribed ranges of 60 the four K fluxes tested in our Monte Carlo simulations were based on previous estimates in 61 literature (Li et al., 2019a and references therein), the range of $\Delta_{\text{sw-sed}}$ was based on field 62 observations (Santiago Ramos et al., 2018; Li et al., 2019a), and the range of $\Delta_{\text{sw-alt}}$ was based on 63 the estimates from this study. Model results are shown in (A), (B), and (C). The range of y-axis 64 shown in (A), (B), and (C) is equivalent to the range tested in the Monte Carlo simulations for 65 F_{MOR} , F_{sed} , and Δ_{sw-sed} , respectively. Blue dots in all three plots are model solutions that 66 simultaneously satisfy K concentration and isotope mass balance. It is obvious that plausible 67 solutions for the three fluxes (F_{MOR} , F_{sed} , and Δ_{sw-sed}) fall within considerably narrower ranges 68 compared to the prescribed ranges tested in Monte Carlo simulations. In (A) and (B), x-axis shows the prescribed range tested in the Monte Carlo simulations for Friv and Falt, respectively. 69

However, these two fluxes are not sensitive to the model as shown in the two plots, and, therefore, estimates of these two fluxes cannot be further refined using our approach. In (C), x-axis shows the refined range of F_{sed} , and no valid solutions can be found outside this refined F_{sed} range.

Fig 5. Modeled δ^{41} K and 87 Sr/ 86 Sr co-variations assuming different Ordovician seawater δ^{41} K values (grey and blue squares), plotted against δ^{41} K results (yellow circles) from ~485 Ma ophiolite (Parendo et al., 2017). Both models used a conservative K isotope fractionation factor ($\Delta_{\text{sw-alt}}$) of -0.2% estimated from this study, and all other parameters were the same as those used in Parendo et al. (2017). Compared to Model 1 that assumed a modern seawater δ^{41} K value of 0.10% for Ordovician seawater (grey curve), a better model—data fit was achieved when seawater δ^{41} K value was assumed to be -0.15% (Model 2, blue curve), ~0.3% lower than the value of modern seawater.

Fig. 1

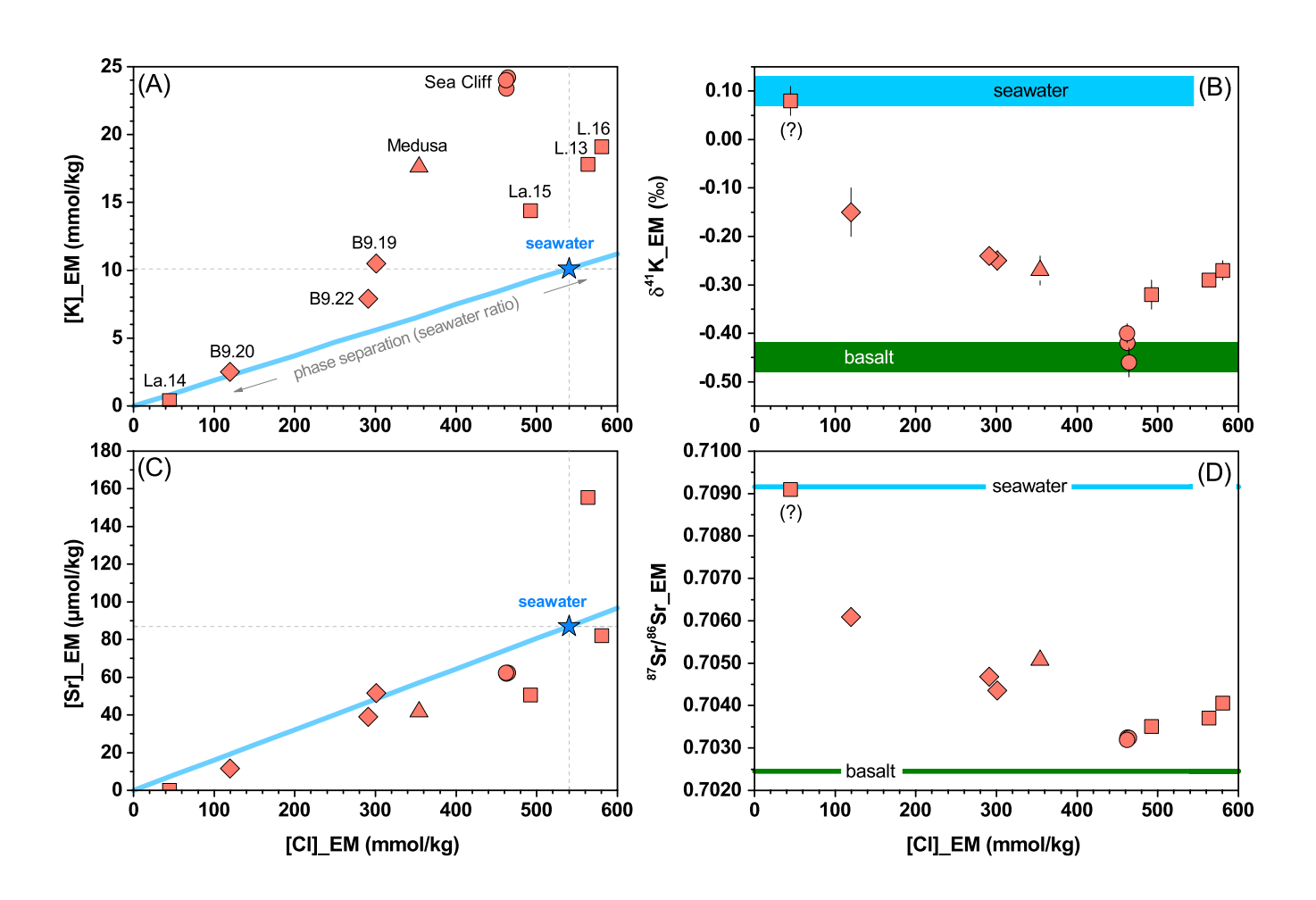


Fig. 2

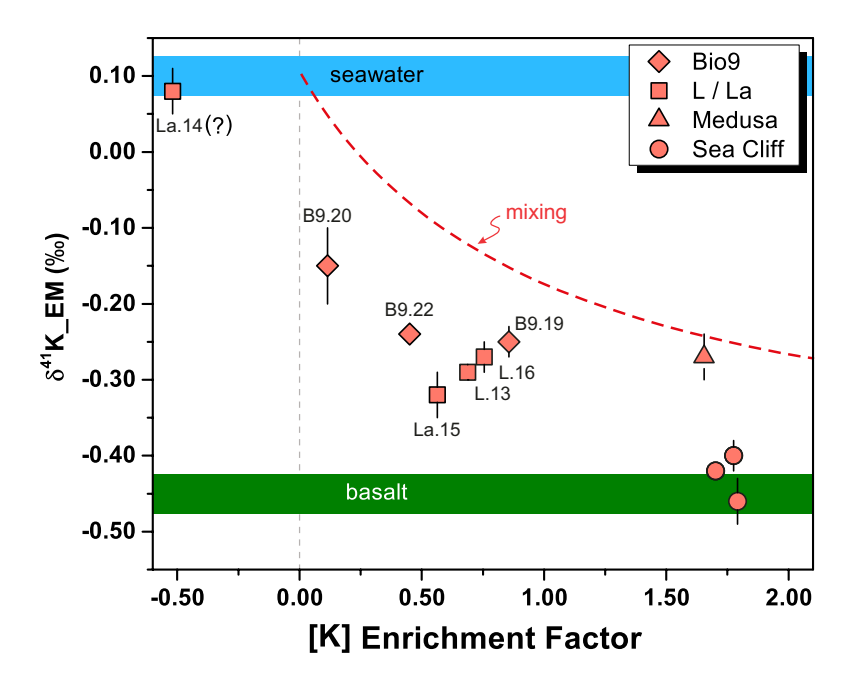
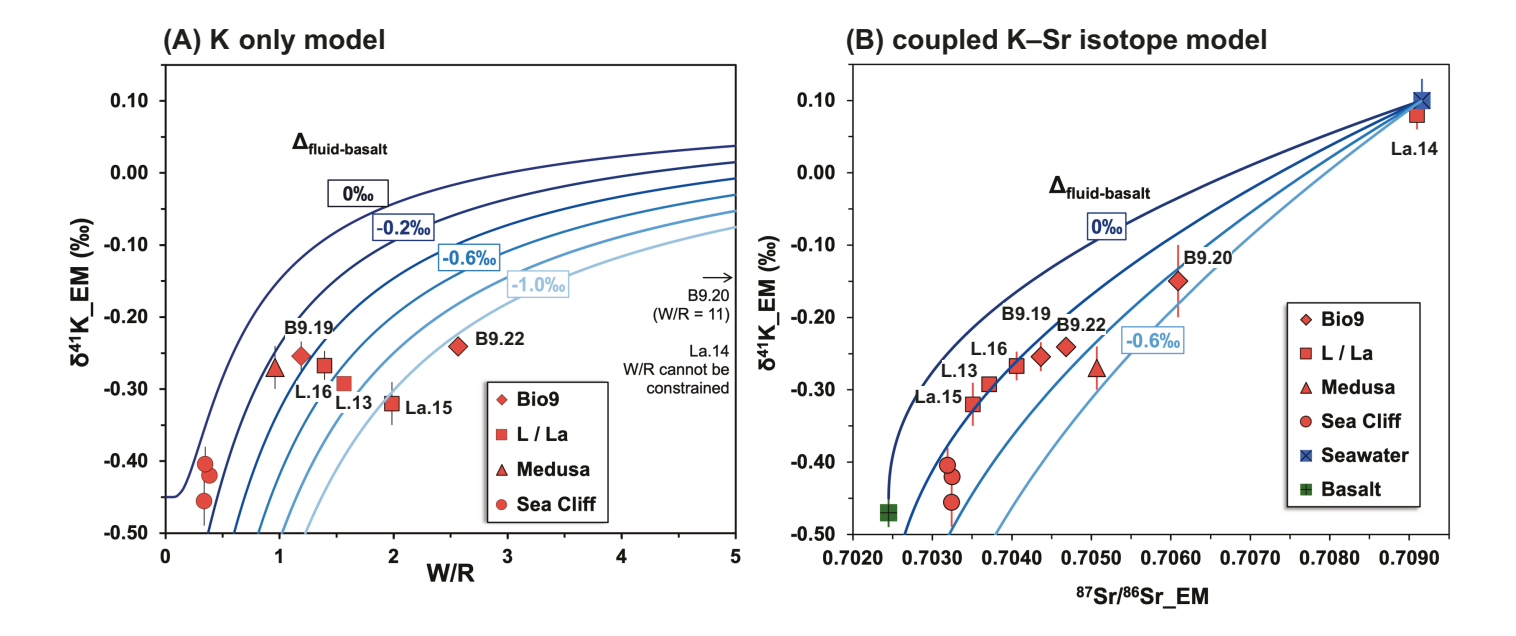


Fig. 3



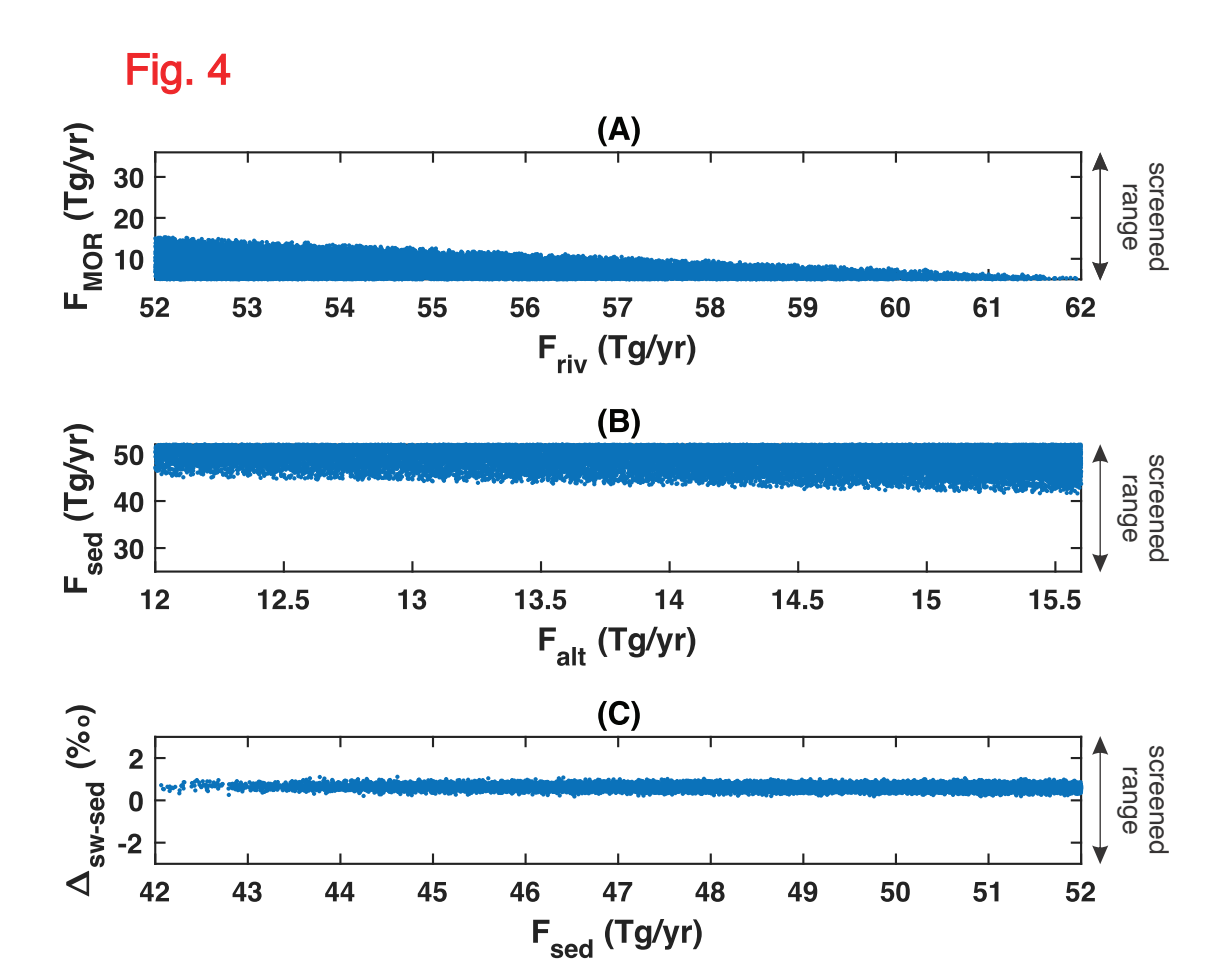
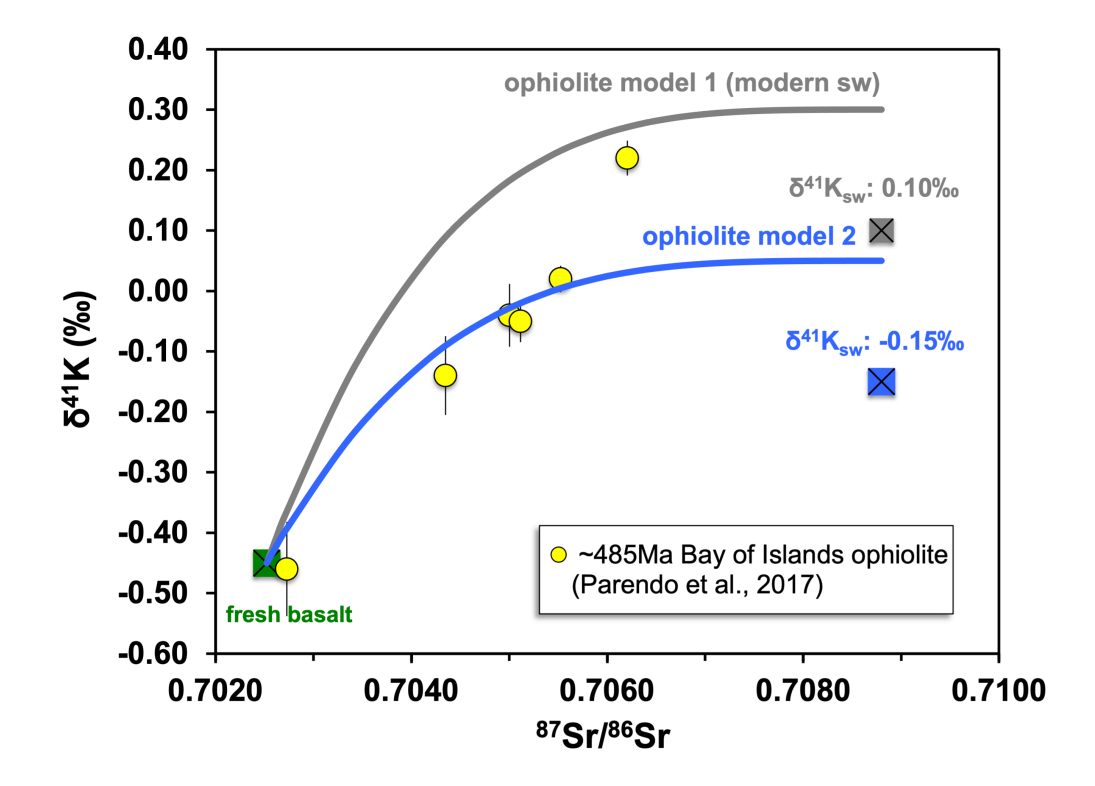


Fig. 5



Appendix

Stable potassium (K) isotope characteristics at mid-ocean ridge hydrothermal vents and its implications for the global K cycle

Xin-Yuan Zheng^{a,1}, Brian L Beard^b, Mason Neuman^b, Maria F Fahnestock^c, Julia G Bryce^c, Clark M. Johnson^b

^a Department of Earth and Environmental Sciences, University of Minnesota–Twin Cities, 116 Church Street SE, Minneapolis MN 55455, USA

^b Department of Geoscience, University of Wisconsin–Madison, 1215 W Dayton Street, Madison WI 53706, USA

^c Department of Earth Sciences, University of New Hampshire, 56 College Road, NH 03824, USA

E-mail address: <u>zhengxy@umn.edu</u> (X.-Y. Zheng)

Phone: +1 612-301-3836

Department of Earth and Environmental Sciences, University of Minnesota-Twin Cities, 150 John Tate Hall, 116 Church Street SE, Minneapolis MN 55455, USA

¹ Corresponding author.

Content

Text

- (1) Data quality control on K isotope measurements
- (2) Derivation of the open system water—rock interaction models based on K concentrations and the coupled K—Sr isotope co-variations
- (3) Choices of input parameters in the water–rock interaction models and results of sensitivity tests
- (4) Mass balance model for the global K cycle in the modern ocean

Figures

- Fig. S1. A map showing sample locations
- **Fig. S2.** δ^{41} K results from 3 test solutions (data quality control)
- Fig. S3. Endmember δ^{41} K values obtained from different sampling bottles (data quality control)
- **Fig. S4.** Sensitivity tests for the K-only model using different D_K values
- Fig. S5. Sensitivity tests for the coupled K-Sr isotope model using different D_K and D_{Sr} values
- **Fig. S6.** Sensitivity tests for the coupled K-Sr isotope model using different q values
- Fig. S7. Monte Carlo simulation results using a larger prescribed F_{alt} range

Tables

- **Table S1.** Results of δ^{41} K, 87 Sr/ 86 Sr, and other relevant physical and chemical measurements
- **Table S2.** Endmember fluid compositions and W/R estimates
- **Table S3.** A summary of input parameters used in the K-only and coupled K-Sr isotope models

Table S4. The elution protocol of column chemistry used to purify K for high-precision isotope analysis in this study

Table S5. Compositions of the three synthetic hydrothermal fluid test solutions prepared to validate our K isotope analysis

(1) Data quality control on K isotope measurements

High-precision stable K isotope (41K/39K) measurements are notoriously challenging due to intense interferences from argon hydride (⁴⁰Ar¹H⁺) on ⁴¹K⁺ and possible tailing from the large ⁴⁰Ar⁺ beam on the adjacent ³⁹K⁺ and ⁴¹K⁺ on the mass spectrometer. In this study, K isotopes were analyzed on a collision-cell equipped MC-ICP-MS (Micromass IsoProbe) in the Department of Geoscience, University of Wisconsin-Madison, following the method reported in Li et al. (2016) with the exception that an Aridus II desolvating unit was used in this study. Interferences on K isotopes from plasma-derived Ar species, notably ⁴⁰Ar¹H⁺ and the tailing of ⁴⁰Ar⁺, were reduced to a negligible level by using helium (He) and deuterium (D₂) as the collision/reaction gas in a hexapole collision cell using settings similar to those reported in Li et al. (2016). Typical K background in blank 2% HNO₃ was ~25 mV (reported on the scale of 10¹¹ohm resistors). Typical K sensitivity was ~4.5 V/ppm, which is similar to the sensitivity reported by a previous study that used a desolvator (i.e., Apex) sample introduction method ("dry plasma") on IsoProbe for K isotope analysis (Wang and Jacobsen, 2016). During the analysis, 4 ppm K solutions were used, yielding signal to background ratios of >650. Background was corrected by an on-peak zero protocol where background K intensities were first measured in blank 2% HNO₃ and then subtracted from the intensities measured in the subsequent sample measurement. Potassium isotopes were analyzed by a sample-standard bracketing protocol. A

pure K solution from High-Purity Standards was used as the in-house bracketing standard, and this solution was routinely analyzed against NIST SRM 3141a, allowing for conversion of K isotope data to the NIST 3141a scale. All δ^{41} K data reported here were on the NIST SRM 3141a scale.

Extensive tests were conducted during the course of this study to ensure data quality. The results of these tests allowed for a critical assessment on accuracy and precision of our K isotope analysis. First, aliquots from each of the three reference materials, BCR-2, BHVO-2, and a natural seawater sample, were processed through column chemistry during the course of this study and each aliquot was analyzed 4-6 times. The natural seawater sample was collected from 500 m at the SEATS site in the South China Sea (Wong et al., 2007). The δ^{41} K results yielded - 0.41 ± 0.04 % (2SE, n = 16) for BCR-2, and 0.10 ± 0.03 % (2SE, n = 12) for seawater, where n represents the total number of analyses. Variability in mean δ^{41} K results obtained from different aliquots was 0.07% (2SD, 3 aliquots) for BCR-2 and 0.05% (2SD, 3 aliquots) for seawater. BHVO-2 was only processed once during this study, and yielded -0.40 ± 0.07 % (2SE, n = 3). All these values agree well with those published from other labs (Wang et al., 2021b).

Second, given the fact that chemical compositions of the three reference materials do not sufficiently match matrices of hydrothermal fluids, we also processed and analyzed three test solutions that mimicked fluid compositions to (1) demonstrate the absence of matrix effects, and (2) better estimate analytical precision and accuracy of our K isotope measurements on fluid samples. We first compiled K to major- and trace-element concentration ratios (K/element) in typical mid-ocean ridge hydrothermal fluids from literature, including chemical data of our fluid samples. Based on these estimated K/element ranges, high-purity single element standards (e.g., Na, Ca, Mg, Si, Rb) were mixed to produce 3 test solutions – one solution with high K/element

ratios (test solution A), one with average K/element ratios (test solution B), and one with low K/element ratios (test solution C). A high-purity K solution with a known δ^{41} K value was used as the K source for the three test solutions. As a result, test solutions A through C had progressively more challenging matrices, and should cover the full range of chemical compositions expected in our fluid samples. In particular, we consider solution C to be a worst-case scenario for fluid samples processed in this study, because it was made to have a combination of low K/element ratios for all major- and trace-elements as defined by extreme values reported for mid-ocean ridge hydrothermal fluids from a wide range of localities in literature, and such an extreme composition is unlikely to be encountered in any individual fluid sample. Test solution compositions were tabulated in Table S5.

A total of 7 separate aliquots from the three test solutions (2-3 from each) were processed through column chemistry and each aliquot was analyzed multiple times during the course of this study. The pooled $\delta^{41}K$ result yielded an overall 2SE of 0.02‰, and was accurate within uncertainty (i.e., matching the known $\delta^{41}K$ value of the high-purity K solution), precluding an influence of matrix effects (Fig. S2). Aliquot-to-aliquot variability was 0.05‰ (2SD), and the worst reproducibility of 0.05‰ was obtained on the test solution C that had matrices more challenging than any sample we analyzed. We considered the results from these test solutions to be more representative to our fluid data because of more pertinent matrices, and we took the precision of 0.05‰ as an upper limit of our K isotope analysis.

Third, we further evaluated our analytical precision through processing 2 separate aliquots of 5 fluid samples through column separation for analysis. Although it is not statistically meaningful to consider the standard deviation on the results from two aliquots, we noticed that the difference in δ^{41} K values obtained from two full-protocol replicates was smaller than 0.05‰

for 4 out 5 replicates (Table S1). These results implied that the precision of our K isotope analysis on actual samples was most likely to be at the level of 0.05‰ or better.

Lastly, besides the tests described above, for all EPR and Medusa vent sites (i.e., 7 out of a total of 11 individual sample collections), we intentionally processed and analyzed two fluid samples taken from two separate sampling bottles for each site, because we were cautious about sampling artifacts and end-member calculations that could inevitably include analytical uncertainties not only associated with K isotope analysis but also K and Mg concentration analysis. We processed each of these fluids separately for isotope analysis, and calculated endmember $\delta^{41}K$ values based on data for individual samples. A comparison of results showed that separately acquired endmember $\delta^{41}K$ values all agreed within 0.02% (Fig. S3). These samples were processed separately through column chemistry, and many of them were analyzed on MC-ICP-MS during different days, so it is unlikely that the good reproducibility reflects a systematic bias on our measurements. These results strongly imply that we were able to reproduce endmember $\delta^{41}K$ values to a ~0.02% level.

(2) Derivation of the open system water—rock interaction models based on K concentrations and the coupled K-Sr isotope co-variations

Similar to the approach used in previous studies (e.g., Spivack and Edmond, 1987; Magenheim et al., 1995; Foustoukos et al., 2004), an open system single-pass water–rock interaction model was developed by assuming incremental additions of fresh basalt in fluid. Chemical compositions of the fluid are evolving in response to addition of fresh basalt at each model step. A mass balance equation can be written for each model step where fresh basalt is incrementally added to chemically evolving fluids:

$$W \times C_f^i + dR \times C_r^i = W \times C_f^{i+1} + dR \times C_r^{i+1}$$
 (Eq. S1)

where W and C_f represent the mass of fluid and [K] concentration in fluid, respectively; dR and C_r denote the mass of each rock increment and [K] content in rock, respectively; and i and i+1 denote the status before and after water–rock equilibration. Assuming a potassium partitioning coefficient between rock and fluid D (= C_r / C_f), and taking initial conditions $C_f^0 = C_{sw}$ and $C_r^0 = C_{basalt}$, integration of the above equation yielded the relation between fluid [K] concentration and W/R ratio:

$$\frac{1}{(W/R)_K} = -\frac{1}{D_K} \ln \left(\frac{C_{basalt} - D_K C_f}{C_{basalt} - D_K C_{sw}} \right) (Eq. S2)$$

Similarly, an isotope mass balance equation can be written for the system as below:

$$W \times C_f^i \times \delta_f^i + dR \times C_r^i \times \delta_r^i = W \times C_f^{i+1} \times \delta_f^{i+1} + dR \times C_r^{i+1} \times \delta_r^{i+1}$$
 (Eq. S3)

where W, C_f , and δ_f represent the mass of fluid, [K] concentration in fluid, and fluid δ^{41} K, respectively; dR, C_r , and δ_r denote the mass of each rock increment, [K] content in rock, and rock δ^{41} K, respectively; and i and i+1 denote the status before and after water–rock equilibration. Assuming a K isotope fractionation factor between fluid and rock Δ_{f-r} (= δ_f – δ_r), and a K partitioning coefficient between rock and fluid D (= C_r / C_f), Eq. (S3) can be rearranged to yield:

$$W \times d\delta_f = D \times (\delta_r^i + \Delta_{f-r} - \delta_f) \times dR$$
 (Eq. S4)

Integrating Eq. (S4)

$$\int_{\delta_f^0}^{\delta_f} \frac{1}{(\delta_r^i + \Delta_{f-r} - \delta_f)} d\delta_f = \int_0^R \frac{D}{W} dR$$

and taking initial conditions $\delta_f^0 = \delta_{sw}$ and $\delta_r^i = \delta_{basalt}$, evolution of fluid K isotope compositions (δ_f) can be then expressed by the following equation:

$$\delta_f = \left(\delta_{basalt} + \Delta_{f-r}\right) - \left(\delta_{basalt} - \delta_{sw} + \Delta_{f-r}\right) \times \exp^{\left(-\frac{D}{W/R}\right)} (Eq. S5).$$

Fluid radiogenic Sr isotopes follow a similar equation as described by Eq. (S5), except for the fact that the fractionation factor between fluid and rock for ⁸⁷Sr/⁸⁶Sr ratios should be zero:

$$^{87}Sr/^{86}Sr_f = ^{87}Sr/^{86}Sr_r - (^{87}Sr/^{86}Sr_r - ^{87}Sr/^{86}Sr_{sw})\exp^{\left(-\frac{D_{Sr}}{W/R}\right)} (Eq. S6)$$

(3) Choices of input parameters in the water—rock interaction models and results of sensitivity tests

Water-rock interaction model results shown in Fig. 3 of the main text were produced using input parameters summarized in Table S3. Seawater $\delta^{41}K_{sw}$ and basalt $\delta^{41}K_{basalt}$ values are based on a compilation of published data for seawater and basalts (Li et al., 2016; Wang and Jacobsen, 2016; Hu et al., 2018; Morgan et al., 2018; Santiago Ramos et al., 2018; Chen et al., 2019; Hille et al., 2019; Tuller-Ross et al., 2019; Xu et al., 2019). Given the restricted ranges reported for the two reservoirs, these two input parameters in the model are well constrained. Radiogenic ⁸⁷Sr/⁸⁶Sr ratios of seawater and MORB are also well constrained; the ratio for seawater was taken from Palmer and Edmond (1989), and the ratio for basalt was based on data reported for MORB samples primarily collected from the areas where our fluid samples were collected (Ito et al., 1987; Davis et al., 2008; Goss et al., 2010; Wanless et al., 2010). It is important to note that ⁸⁷Sr/⁸⁶Sr ratios of basalts from the overlapping spreading center at ~9°N on EPR where the Medusa vent was found are indistinguishable from those measured for MORB from other study areas (Wanless et al., 2010), although lavas found at ~9°N are chemically more evolved (i.e., dacitic) (Wanless et al., 2010; Wanless et al., 2012). Distribution coefficient between basalt and fluid for K, D_K, is based on a compilation of results from hydrothermal alteration experiments conducted at T-P conditions pertinent to MOR hydrothermal systems (Mottl and Holland, 1978; Seyfried et al., 1984; Seyfried et al., 1998), and was found to vary

between \sim 0.1 and \sim 0.6 without obvious temperature dependence at \geq 300°C. An upper limit value of 0.6 was used to produce the results shown in Figure 3 in the main text.

For the K-only model, the main source of uncertainty is choice of D_k . We recognize that considerably lower D_k values (e.g., <0.1), reflecting intense leaching of K from basalt, are possible when comparing K concentrations measured in our fluid samples to K concentrations measured in sheeted dike sampled from the nearby DSDP 504B drill core (Alt et al., 1986; Bach et al., 2003). We tested the influence of lower D_k values on estimation of the apparent K isotope fractionation in the K-only model, and we found that a lower D_k value leads to quantification of even larger K isotope fractionation (Fig. S4). The results shown in the main text are therefore conservative estimates. Our use of a higher D_K value of 0.6 strikes a balance between K uptake at low temperature and K leaching at high temperature, and it is thus more appropriate for the goal of our model – that is to constrain the net K isotope effect produced over the entire hydrothermal convection path.

For the coupled K–Sr model, relative to D_K , D_{Sr} is less well constrained due to varied anhydrite precipitation in experimental and natural hydrothermal systems, as well as natural variability in mineral Sr contents. Following a previous approach (Parendo et al., 2016), D_{Sr} was assumed to be equal to the initial Sr concentration ratio of local basalts (~100 ppm, (Davis et al., 2008; Goss et al., 2010; Wanless et al., 2012)) and seawater (~87 μ M, (Von Damm, 2000)). Because Sr contents in most of our fluids lie slightly below the seawater [Sr]–[Cl] line shown in Fig. 1C of the main text, implying minor net loss of fluid Sr, our chosen D_{Sr} value is likely an underestimate.

With prescribed D_K and D_{Sr} values, apparent K isotope fractionation $\Delta^{41}K_{fluid-basalt}$ can be quantified using Eqs. S5 and S6 (i.e., Eqs. (1) and (3) in the main text). Assuming a common

W/R ratio in this coupled model, a logical initial assumption, could lead to an estimate of unrealistically large K isotope fractionation (i.e., \leq -5%). This reflects the fact that the W/Rratio is an element-specific parameter closely related to chemical behavior of individual element during hydrothermal alteration. For example, because Sr is typically less fluid mobile relative to alkali elements including K during high-temperature hydrothermal alteration, it is well known that a W/R ratio calculated based on fluid ${}^{87}Sr/{}^{86}Sr$ would give a higher value (i.e., "less altered") than that calculated based on alkali elements for the same hydrothermal system (e.g., Berndt et al., 1988). Consequently, it is more appropriate to assume different W/R ratios for K and Sr in a coupled geochemical model. A scale factor q, such that $(W/R)_K = q(W/R)_{Sr}$, can be used to take account of different reactivity of K and Sr during hydrothermal alteration, and this approach was used in a previous study (e.g., McCulloch et al., 1981). Fluid ⁸⁷Sr/⁸⁶Sr values allow for direct calculation of $(W/R)_{Sr}$ using the water–rock interaction model (Eq. S6), and typically yielded values ranging from ~6 to ~14 (Table S2). Data from "time-zero" fluids collected immediately after the volcanic eruption in 2006 (B9.20 and La.14) were calculated to give much higher W/R ratios that are likely transient signals. $(W/R)_K$ ratios were estimated to range between ~0.3 and ~11 using Eq. S2 (Table S2). This method cannot provide a W/R estimate for the time-zero fluid La.14, because its [K] concentration showed a deficiency relative to that of seawater on a [C1]-normalized basis. Based on independent constraints on $(W/R)_{Sr}$ and $(W/R)_K$ (Table S2), values of the scale factor q can be estimated to range between ~0.07 and ~0.5 for vents at EPR, and at slightly lower values of ~ 0.06 for vents from the Gorda Ridge. A q value of 0.1 was taken as a representative value to produce results shown in Fig. 3B of the main text, because this value is close to both the average and median value of q estimates for all vents studied here.

Major uncertainties in the coupled K-Sr model come from input values for Dk, DSr, and the scale factor q. We conducted a series of sensitivity experiments to explore the influence of these parameters on quantification of the apparent K isotope fractionation. Similar to the K-only model, assuming all other parameters in the model unchanged, we found that a smaller D_K value could shift the modeled $\delta^{41}K^{-87}Sr/^{86}Sr$ curve towards the upper left corner in the $\delta^{41}K^{-87}Sr/^{86}Sr$ space (Fig. S5), making it more difficult to fit model results to observational data, unless a more negative Δ^{41} K_{fluid-basalt} is used. As discussed above, our chosen D_{Sr} value of ~13 is likely to be an underestimate. Assuming all other parameters in the model unchanged, a larger D_{Sr} value could shift the modeled $\delta^{41}K^{-87}Sr/^{86}Sr$ curve towards the upper left corner in the $\delta^{41}K^{-87}Sr/^{86}Sr$ space (Fig. S5), making it more difficult to fit model results to observational data, unless a more negative Δ^{41} K_{fluid-basalt} is used. Again, like our choice for D_K value, the D_{Sr} value used to produce the results shown in Figure 3B of our main text provided a conservative constraint on the minimum magnitude of K isotope fractionation. In addition, we also tested the influence of different q values on the model output. Using a q value of 0.07, a lower limit for vents at EPR, estimates of Δ^{41} K_{fluid-basalt} ranged between ~ -0.1‰ and ~ -0.3‰ (Fig. S6). Using a q value of 0.06, a lower limit constrained for the vents on the Gorda Ridge, the estimated $\Delta^{41}K_{fluid-basalt}$ for MOR vents on the Gorda Ridge is \sim -0.1%. Using an upper limit of 0.5 for q would yield unrealistically large magnitude of K isotope fractionation between fluid and basalt (Fig. S6). Although uncertainties are inevitable, it is clear that, even based on some extreme input values, fitting of the model to observational data always predicts a preferential enrichment in light K isotopes in fluid relative to basalt.

(4) Mass balance model for the global K cycle in the modern ocean

Mass-balance equations for K fluxes and isotopes in the ocean can be written as:

$$F_{riv} + F_{MOR} = F_{alt} + F_{sed} (\textbf{\textit{Eq.S7}})$$

$$\delta^{41}K_{riv}F_{riv} + \delta^{41}K_{MOR}F_{MOR} = \delta^{41}K_{alt}F_{alt} + \delta^{41}K_{sed}F_{sed} (\textbf{\textit{Eq.S8}})$$

Two K isotope fractionation factors $\Delta_{\text{sw-sed}}$ (= $\delta^{41}K_{\text{sw}} - \delta^{41}K_{\text{sed}}$) and $\Delta_{\text{sw-alt}}$ (= $\delta^{41}K_{\text{sw}} - \delta^{41}K_{\text{alt}}$) can be introduced into the model via Eq. S8. Previous estimates based on K concentrations are often associated with large uncertainties for many terms in the above equations; estimated F_{MOR} , F_{sed} , F_{riv} , and F_{alt} fluxes ranged from 5 to 36 Tg/yr, from 25 to 52 Tg/yr, from 52 to 62 Tg/yr, and from 12 to 15.6 Tg/yr, respectively. The estimated $\delta^{41}K_{riv}$ for the global riverine input ranges between ~-0.2% and ~-0.4% (Li et al., 2019; Wang et al., 2021a). The estimated ranges for all parameters in literature are large, but K isotope mass balance provides an additional constraint on the global K cycle that was not possible at the time previous estimates were made, and hence should improve those previous estimates. A Monte Carlo approach was used to refine estimates on various K fluxes and K isotope fractionation factors in the modern ocean. Compared to previous studies, our work provided new constraints on $\delta^{41}K_{MOR}$ (-0.32 ± 0.08 %) and Δ_{sw-alt} (- $0.2\% \sim -0.5\%$) that were not known until our study. The large range from -3% to +3% was set for $\Delta_{\text{sw-sed}}$ in the Monte Carlo experiments. Each simulation randomly selected input values within the prescribed ranges mentioned above, and then the input values were tested to check if they fulfil the two mass balance equations (Eq. S7 and S8). Solutions that can simultaneously fulfil the two mass balance equations are accepted otherwise rejected. A total of two billion Monte Carlo experiments were conducted, and it was found that F_{MOR} , F_{sed} , and Δ_{sw-sed} could be considerably refined as compared to the large ranges prescribed for the simulations. F_{MOR} was estimated to range between 5 and 15.3 Tg/yr, and F_{sed} was estimated to range between 42 to 52 Tg/yr. Although an unrealistically large range between -3% and +3% range was prescribed for

 $\Delta_{\text{sw-sed}}$ in the Monte Carlo simulations, experiment results indicated that $\Delta_{\text{sw-sed}}$ must be 0.53 \pm 0.06‰ (1 s.d.) in order to meet the two mass-balance constraints, confirming that our simulations captured the entire possible range. F_{riv} , and F_{alt} are not sensitive in the model, so they cannot be further constrained with existing data.

Recent studies suggested the possibility for a considerably higher F_{alt} (Coogan and Gillis, 2018). We tested the influence of a higher F_{alt} on our model results by increasing the upper limit of F_{alt} to 30 Tg/yr (i.e., ~2-time the current upper limit) while keeping all other inputs unchanged. A total of 200 million Monte Carlo simulations were conducted, and the results are shown in Fig S7. The results show that the possible K sedimentary flux F_{sed} still occupied the upper area of the prescribed range, which is consistent with the trend presented in the main text, although the possible ranges for F_{MOR} and F_{sed} are slightly larger. This result indicates the need for an improved estimate for F_{alt} to more accurately quantify the K flux associated with the sedimentary removal.

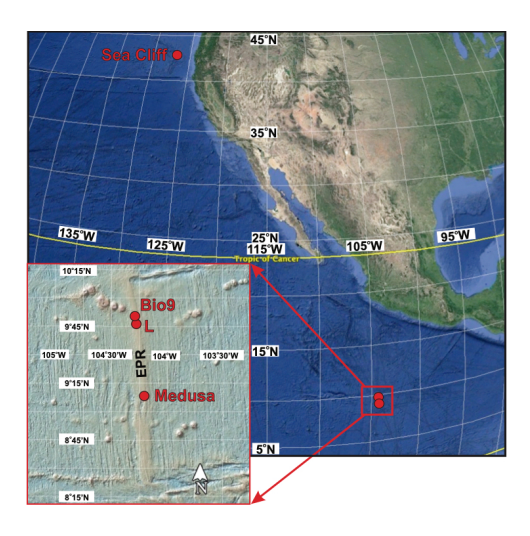


Fig. S1 A map of sample locations

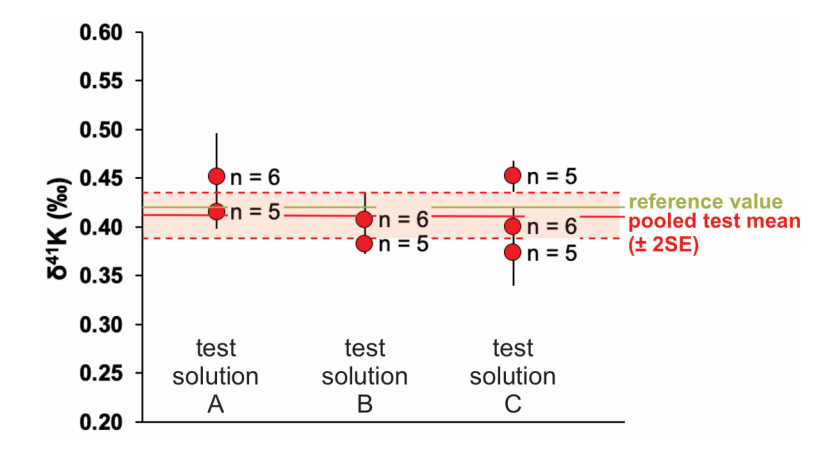


Fig. S2 δ^{41} K results measured for the three synthetic hydrothermal fluid test solutions.

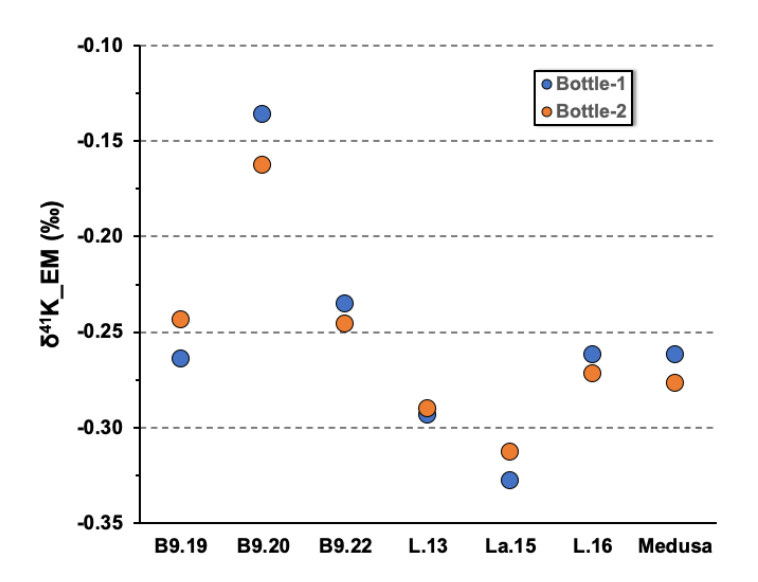


Fig. S3 Calculated endmember $\delta^{41}K$ values based on analyses of samples from two different sampling bottles for 7 individual sample collections. It is important to note that endmember $\delta^{41}K$ values derived from individual measurements of samples from two bottles of the same vent all agreed within 0.02‰.

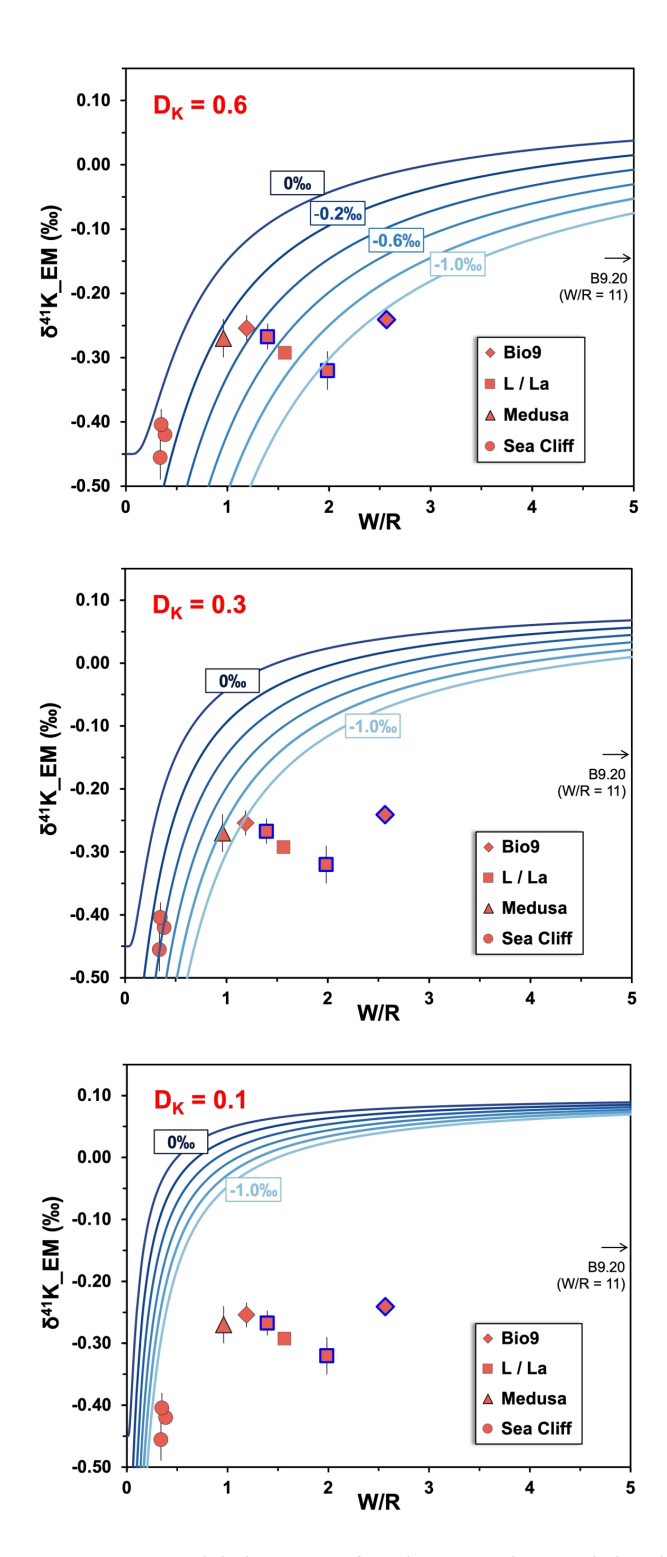


Fig. S4 Sensitivity tests for the K-only model using different D_K values. It can be seen from these results that a smaller D_K would constrain larger K isotope fractionation. Sample symbols with blue edges are those strongly affected by the volcanic eruption.

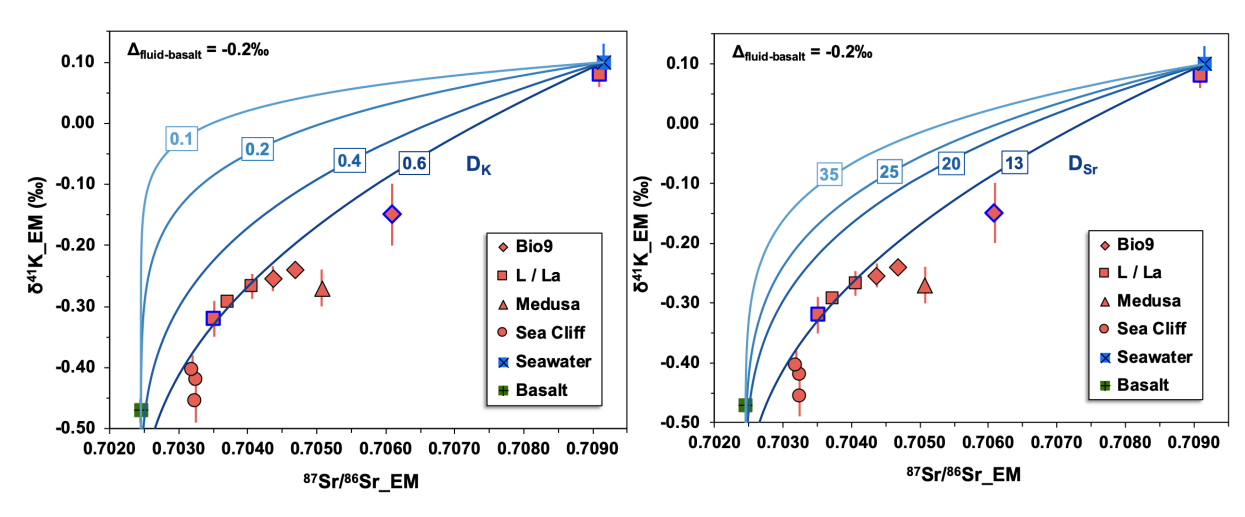


Fig. S5 Sensitivity test results of the modeled δ^{41} K $^{-87}$ Sr $^{/86}$ Sr curves as a function of different D_K (left) and D_{Sr} (right), plotted against observational data. A constant Δ^{41} K $_{fluid-basalt}$ value of -0.2‰ was chosen for the purpose of illustration here. It can be seen that lower D_K , or larger D_{Sr} , would shift the model curve away from observational data, making it harder to achieve a good fit between the model and data unless a Δ^{41} K $_{fluid-basalt}$ value more negative than -0.2‰ is used. These results suggest that a D_K value of 0.6 and a D_{Sr} value of 13 used to produce the results shown in the main text provided a conservative constraint on the minimum magnitude of K isotope fractionation between fluid and basalt. Sample symbols with blue edges are those strongly affected by the volcanic eruption.

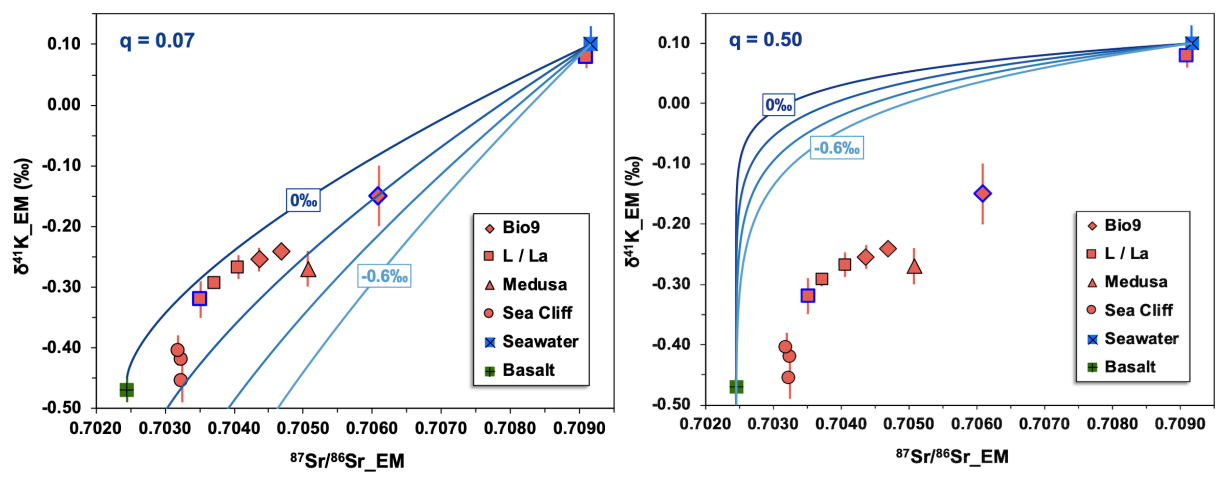


Fig. S6 Sensitivity test results showing the modeled $\delta^{41}K^{-87}Sr/^{86}Sr$ curves using two different values for the scale factor q, plotted against observational data. The plot on the left used a q value of 0.07 that is the lower limit of q, and the plot on the right used an upper limit q value of 0.5. Dark to light blue curves in both plots represent different $\Delta^{41}K_{fluid-basalt}$ values between - 0.6% and 0% with an increment of 0.2%. It shows that a larger q would result in a more negative $\Delta^{41}K_{fluid-basalt}$ value, and an extreme value of 0.07 would suggest $\Delta^{41}K_{fluid-basalt}$ values ranging between \sim -0.1% and \sim -0.3%. A more moderate q value of 0.1 that is close to both the mean and median value estimated for all fluids analyzed in this study was used to compute the results reported in the main text. Sample symbols with blue edges are those strongly affected by the volcanic eruption.

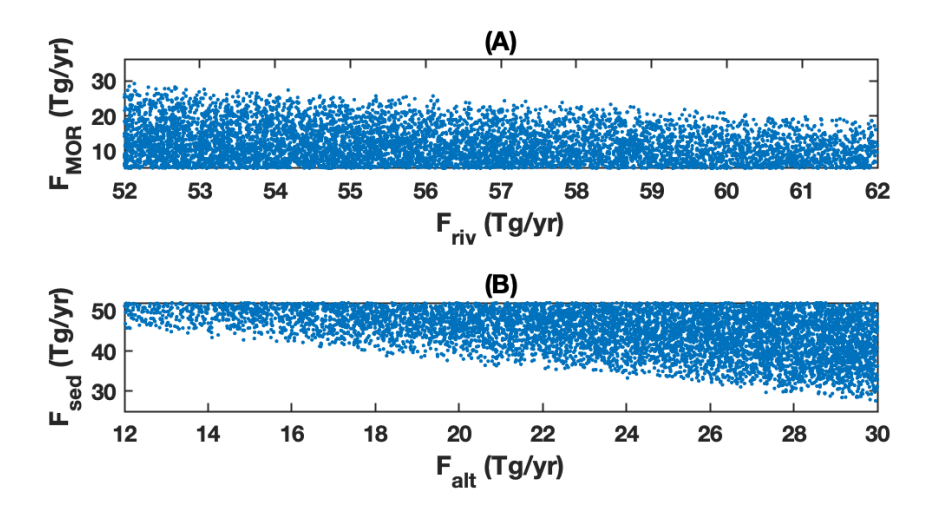


Fig. S7 Sensitivity test results using a larger prescribed range for F_{alt} (12-30 Tg/yr) to account for a possible larger K removal flux associated with low-temperature hydrothermal alteration. The range of x- or y- axis shown in this figure is the prescribed range for the corresponding parameter tested in the Monte Carlo simulations, and 200 million simulations were conducted. Blue dots represent valid model solutions. Although the possible ranges of F_{MOR} and F_{sed} that fulfil the coupled K elemental and isotope mass balance are different from the possible ranges resulting from the use of a narrower F_{alt} input range (12-15.5 Tg/yr), the trend that valid F_{sed} fluxes occupy the upper area of the prescribed estimates remains unchanged.

References

- Alt J. C., Honnorez J., Laverne C. and Emmermann R. (1986) Hydrothermal alteration of a 1 km section through the upper oceanic crust, Deep Sea Drilling Project Hole 504B: Mineralogy, chemistry and evolution of seawater-basalt interactions. *Journal of Geophysical Research: Solid Earth* **91**, 10309-10335, 10.1029/JB091iB10p10309.
- Avigad D., Sandler A., Kolodner K., Stern R. J., McWilliams M., Miller N. and Beyth M. (2005) Mass-production of Cambro—Ordovician quartz-rich sandstone as a consequence of chemical weathering of Pan-African terranes: Environmental implications. *Earth and Planetary Science Letters* **240**, 818-826, https://doi.org/10.1016/j.epsl.2005.09.021.
- Bach W., Peucker-Ehrenbrink B., Hart S. R. and Blusztajn J. S. (2003) Geochemistry of hydrothermally altered oceanic crust: DSDP/ODP Hole 504B Implications for seawater-crust exchange budgets and Sr- and Pb-isotopic evolution of the mantle. *Geochemistry, Geophysics, Geosystems* **4**, 10.1029/2002gc000419.
- Berndt M. E., Seyfried W. E. and Beck J. W. (1988) Hydrothermal alteration processes at midocean ridges: Experimental and theoretical constraints from Ca and Sr exchange reactions and Sr isotopic ratios. *Journal of Geophysical Research: Solid Earth* **93**, 4573-4583, 10.1029/JB093iB05p04573.
- Berner R. A. and Kothavala Z. (2001) Geocarb III: A Revised Model of Atmospheric CO2 over Phanerozoic Time. *Am. J. Sci.* **301**, 182-204, 10.2475/ajs.301.2.182.
- Bryce, J. G., Prado, M. F., Bryce, J. G. (2011) Hydrothermal Vent Fluid Geochemistry, AT15-17, Version 1.0. Earth Data Alliance (IEDA). https://doi.org/10.1594/IEDA/100031.
- Bryce J, Prado F, Von Damm K, (2015a) Vent Fluid Chemistry Data from samples acquired with HOV Alvin during the Atlantis expedition AT11-20 (2004) at the East Pacific Rise at 9N. Integrated Earth Data Applications (IEDA). https://doi.org/10.1594/IEDA/317362.
- Bryce J, Prado F, Von Damm K (2015b) Vent Fluid Chemistry Data, including Metals Fractions and Dissolved Majors, from fluid samples acquired with HOV Alvin during Atlantis expedition AT15-13 (2006) at the East Pacific Rise at 9N. Integrated Earth Data Applications (IEDA). https://doi.org/10.1594/IEDA/317364.
- Bryce J, Prado F, Von Damm K. (2015c) Vent Fluid Chemistry Data, including Metals Fractions and Dissolved Majors, from fluid samples acquired with HOV Alvin during Atlantis expedition AT15-06 (2006) at the East Pacific Rise at 9N. Integrated Earth Data Applications (IEDA). https://doi.org/10.1594/IEDA/317365.
- Bryce J, Prado F, Von Damm K. (2015d) Vent Fluid Chemistry Data, including Metals Fractions and Dissolved Majors, from fluid samples acquired with HOV Alvin during Atlantis expedition AT15-27 (2007) at the East Pacific Rise at 9N. Integrated Earth Data Applications (IEDA). https://doi.org/10.1594/IEDA/317603.
- Chen H., Tian Z., Tuller-Ross B., Korotev Randy L. and Wang K. (2019) High-precision potassium isotopic analysis by MC-ICP-MS: an inter-laboratory comparison and refined K atomic weight. *Journal of Analytical Atomic Spectrometry* 10.1039/C8JA00303C.
- Coogan L. A. and Gillis K. M. (2018) Low-Temperature Alteration of the Seafloor: Impacts on Ocean Chemistry. *Annual Review of Earth and Planetary Sciences* **46**, 21-45, 10.1146/annurev-earth-082517-010027.
- Davis A. S., Clague D. A., Cousens B. L., Keaten R. and Paduan J. B. (2008) Geochemistry of basalt from the North Gorda segment of the Gorda Ridge: Evolution toward ultraslow

- spreading ridge lavas due to decreasing magma supply. *Geochemistry, Geophysics, Geosystems* **9**, 10.1029/2007GC001775.
- Foustoukos D. I., James R. H., Berndt M. E. and Seyfried W. E. (2004) Lithium isotopic systematics of hydrothermal vent fluids at the Main Endeavour Field, Northern Juan de Fuca Ridge. *Chemical Geology* **212**, 17-26, https://doi.org/10.1016/j.chemgeo.2004.08.003.
- Gaffin S. (1987) Ridge volume dependence on seafloor generation rate and inversion using long term sealevel change. *Am. J. Sci.* **287**, 596-611, 10.2475/ajs.287.6.596.
- Goss A. R., Perfit M. R., Ridley W. I., Rubin K. H., Kamenov G. D., Soule S. A., Fundis A. and Fornari D. J. (2010) Geochemistry of lavas from the 2005-2006 eruption at the East Pacific Rise, 9° 46′ N-9° 56′ N: Implications for ridge crest plumbing and decadal changes in magma chamber compositions. *Geochemistry, Geophysics, Geosystems* 11, doi:10.1029/2009GC002977.
- Hardie L. A. (1996) Secular variation in seawater chemistry: An explanation for the coupled secular variation in the mineralogies of marine limestones and potash evaporites over the past 600 m.y. *Geology* **24**, 279-283, 10.1130/0091-7613(1996)024<0279:svisca>2.3.co;2.
- Hille M., Hu Y., Huang T.-Y. and Teng F.-Z. (2019) Homogeneous and heavy potassium isotopic composition of global oceans. *Science Bulletin* https://doi.org/10.1016/j.scib.2019.09.024.
- Hu Y., Chen X. Y., Xu Y. K. and Teng F. Z. (2018) High-precision analysis of potassium isotopes by HR-MC-ICPMS. *Chemical Geology* **493**, 100-108, 10.1016/j.chemgeo.2018.05.033.
- Ito E., White W. M. and Göpel C. (1987) The O, Sr, Nd and Pb isotope geochemistry of MORB. *Chemical Geology* **62**, 157-176, https://doi.org/10.1016/0009-2541(87)90083-0.
- Lenton T. M., Daines S. J. and Mills B. J. W. (2018) COPSE reloaded: An improved model of biogeochemical cycling over Phanerozoic time. *Earth-Science Reviews* **178**, 1-28, https://doi.org/10.1016/j.earscirev.2017.12.004.
- Li S., Li W., Beard B. L., Raymo M. E., Wang X., Chen Y. and Chen J. (2019) K isotopes as a tracer for continental weathering and geological K cycling. *Proceedings of the National Academy of Sciences* 201811282, 10.1073/pnas.1811282116.
- Li W., Beard B. L. and Li S. (2016) Precise measurement of stable potassium isotope ratios using a single focusing collision cell multi-collector ICP-MS. *Journal of Analytical Atomic Spectrometry* **31**, 1023-1029, 10.1039/C5JA00487J.
- Mackenzie F. T. and Kump L. R. (1995) Reverse Weathering, Clay Mineral Formation, and Oceanic Element Cycles. *Science* **270**, 586-586, 10.1126/science.270.5236.586.
- Magenheim A. J., Spivack A. J., Alt J. C., Bayhurst G., Chan L., Zuleger E. and Gieskes J. M. (1995) Borehole fluid chemistry in Hole 504b, Leg 137: formation water or in-situ reaction?, Proceedings of the Ocean Drilling Program, Scientific Results, pp. 141-52.
- McArthur J. M., Howarth R. J. and Bailey T. R. (2001) Strontium Isotope Stratigraphy: LOWESS Version 3: Best Fit to the Marine Sr Isotope Curve for 0-509 Ma and Accompanying Look up Table for Deriving Numerical Age. *The Journal of Geology* **109**, 155-170, 10.1086/319243.
- McCulloch M. T., Gregory R. T., Wasserburg G. J. and Taylor H. P. (1981) Sm-Nd, Rb-Sr, and ¹⁸O/¹⁶O isotopic systematics in an oceanic crustal section: evidence from the Samail Ophiolite. *Journal of Geophysical Research: Solid Earth* **86**, 2721-2735, http://dx.doi.org/10.1029/JB086iB04p02721.

- Michalopoulos P. and Aller R. C. (1995) Rapid Clay Mineral Formation in Amazon Delta Sediments: Reverse Weathering and Oceanic Elemental Cycles. *Science* **270**, 614-617, 10.1126/science.270.5236.614.
- Miller K. G., Kominz M. A., Browning J. V., Wright J. D., Mountain G. S., Katz M. E., Sugarman P. J., Cramer B. S., Christie-Blick N. and Pekar S. F. (2005) The Phanerozoic Record of Global Sea-Level Change. *Science* **310**, 1293-1298, 10.1126/science.1116412.
- Morgan L. E., Santiago Ramos D. P., Davidheiser-Kroll B., Faithfull J., Lloyd N. S., Ellam R. M. and Higgins J. A. (2018) High-precision 41 K/ 39 K measurements by MC-ICP-MS indicate terrestrial variability of δ^{41} K. *Journal of Analytical Atomic Spectrometry* **33**, 175-186, 10.1039/C7JA00257B.
- Mottl M. J. and Holland H. D. (1978) Chemical exchange during hydrothermal alteration of basalt by seawater—I. Experimental results for major and minor components of seawater. *Geochimica et Cosmochimica Acta* **42**, 1103-1115, http://dx.doi.org/10.1016/0016-7037(78)90107-2.
- Palmer M. R. and Edmond J. M. (1989) The strontium isotope budget of the modern ocean. *Earth and Planetary Science Letters* **92**, 11-26, http://dx.doi.org/10.1016/0012-821X(89)90017-4.
- Parendo C. A., Jacobsen S. B. and Wang K. (2016) Potassium isotopes as a new tracer of seafloor hydrothermal alteration: the Bay of Islands Ophiolite. *AGU Fall Meeting Abstract*
- Parendo C. A., Jacobsen S. B. and Wang K. (2017) K isotopes as a tracer of seafloor hydrothermal alteration. *Proc Natl Acad Sci U S A* **114**, 1827-1831, 10.1073/pnas.1609228114.
- Qing H., Barnes C. R., Buhl D. and Veizer J. (1998) The strontium isotopic composition of Ordovician and Silurian brachiopods and conodonts: relationships to geological events and implications for coeval seawater. *Geochimica et Cosmochimica Acta* **62**, 1721-1733, https://doi.org/10.1016/S0016-7037(98)00104-5.
- Royer D. L., Donnadieu Y., Park J., Kowalczyk J. and Godderis Y. (2014) Error analysis of CO2 and O2 estimates from the long-term geochemical model GEOCARBSULF. *Am. J. Sci.* **314**, 1259-1283,
- Santiago Ramos D. P., Morgan L. E., Lloyd N. S. and Higgins J. A. (2018) Reverse weathering in marine sediments and the geochemical cycle of potassium in seawater: Insights from the K isotopic composition (⁴¹K/ ³⁹K) of deep-sea pore-fluids. *Geochimica et Cosmochimica Acta* **236**, 99-120, 10.1016/j.gca.2018.02.035.
- Seyfried W. E., Janecky D. R. and Mottl M. J. (1984) Alteration of the oceanic crust: Implications for geochemical cycles of lithium and boron. *Geochimica et Cosmochimica Acta* **48**, 557-569, https://doi.org/10.1016/0016-7037(84)90284-9.
- Seyfried W. E., Chen X. and Chan L.-H. (1998) Trace element mobility and lithium isotope exchange during hydrothermal alteration of seafloor weathered basalt: an experimental study at 350°C, 500 Bars. *Geochimica et Cosmochimica Acta* **62**, 949-960, https://doi.org/10.1016/S0016-7037(98)00045-3.
- Spivack A. J. and Edmond J. M. (1987) Boron isotope exchange between seawater and the oceanic crust. *Geochimica et Cosmochimica Acta* **51**, 1033-1043, https://doi.org/10.1016/0016-7037(87)90198-0.

- Tuller-Ross B., Marty B., Chen H., Kelley K. A., Lee H. and Wang K. (2019) Potassium isotope systematics of oceanic basalts. *Geochimica et Cosmochimica Acta* **259**, 144-154, https://doi.org/10.1016/j.gca.2019.06.001.
- Von Damm K. L. (2000) Chemistry of hydrothermal vent fluids from 9°–10°N, East Pacific Rise: "Time zero," the immediate posteruptive period. *Journal of Geophysical Research: Solid Earth* **105**, 11203-11222, doi:10.1029/1999JB900414.
- Von Damm, K. L., Prado, M. F., Bryce, J. G. (2014) Geochemistry of vents in the Seacliff and Escanaba Hydrothermal Fields (2000 and 2002), Version 1.0. Interdisciplinary Earth Data Alliance (IEDA). https://doi.org/10.1594/IEDA/100414.
- Wang K. and Jacobsen S. B. (2016) An estimate of the Bulk Silicate Earth potassium isotopic composition based on MC-ICPMS measurements of basalts. *Geochimica et Cosmochimica Acta* **178**, 223-232, http://dx.doi.org/10.1016/j.gca.2015.12.039.
- Wang K., Peucker-Ehrenbrink B., Chen H., Lee H. and Hasenmueller E. A. (2021a) Dissolved potassium isotopic composition of major world rivers. *Geochimica et Cosmochimica Acta* **294**, 145-159, https://doi.org/10.1016/j.gca.2020.11.012.
- Wang K., Li W., Li S., Tian Z., Koefoed P. and Zheng X.-Y. (2021b) Geochemistry and cosmochemistry of potassium stable isotopes. *Geochemistry* 125786, https://doi.org/10.1016/j.chemer.2021.125786.
- Wanless V. D., Perfit M. R., Ridley W. I. and Klein E. (2010) Dacite petrogenesis on Mid-Ocean Ridges: evidence for oceanic crustal melting and assimilation. *Journal of Petrology* **51**, 2377-2410, 10.1093/petrology/egq056.
- Wanless V. D., Perfit M. R., Klein E. M., White S. and Ridley W. I. (2012) Reconciling geochemical and geophysical observations of magma supply and melt distribution at the 9°N overlapping spreading center, East Pacific Rise. *Geochemistry, Geophysics, Geosystems* 13, 10.1029/2012gc004168.
- Wong G. T. F., Ku T.-L., Mulholland M., Tseng C.-M. and Wang D.-P. (2007) The SouthEast Asian Time-series Study (SEATS) and the biogeochemistry of the South China Sea—An overview. *Deep Sea Research Part II: Topical Studies in Oceanography* **54**, 1434-1447, https://doi.org/10.1016/j.dsr2.2007.05.012.
- Xu Y.-K., Hu Y., Chen X.-Y., Huang T.-Y., Sletten R. S., Zhu D. and Teng F.-Z. (2019) Potassium isotopic compositions of international geological reference materials. *Chemical Geology* **513**, 101-107, 10.1016/j.chemgeo.2019.03.010.